BMC Biology

RESEARCH

Open Access

p53-mediated suppression of the SLC7 A11/GPX4 signaling pathway promotes trophoblast ferroptosis in preeclampsia

Tingting Liao[1†], Xia Xu[1†], Guiying Wang[1] and Jianying Yan[1*]

Abstract

Background Ferroptosis is an iron-dependent form of non-apoptotic cell death that occurs through increased plasma membrane phospholipid peroxidation in the context of impaired plasma membrane phospholipid peroxide repair systems. It has been reported that p53 can inhibit the expression of cysteine/glutamate reverse transporter solute carrier family 7, member 11 (SLC7A11), a key component of system Xc-, thus inhibiting cysteine uptake and promoting reactive oxygen species (ROS) accumulation as an important part of cell ferroptosis. Preeclampsia (PE) is an idiopathic hypertensive disease of pregnancy. Spiral artery insufficiency and impaired placental development are present at all stages, leading to placental hypoperfusion, ischemia, and hypoxia. However, the role of ferroptosis, particularly p53-mediated trophoblast ferroptosis, in placental dysfunction during PE remains unclear.

Results In PE placental tissues, malondialdehyde (MDA) and total iron levels were elevated, and trophoblasts exhibited typical ferroptosis-associated morphological changes. Additionally, p53 mRNA and protein expression and the percentage of p53-positive cells were increased, while SLC7A11 and GPX4 mRNA and protein expression and the percentage of positive cells were decreased. VEGFR1 protein expression was upregulated, whereas VEGFA and PLGF protein expression was downregulated. p53 protein expression was negatively correlated with the expression of proteins in the SLC7A11/GPX4 signaling pathway, VEGFA, and PLGF. Conversely, there was a positive correlation between p53 expression and MDA, total iron concentration, and VEGFR1.

In vitro, the ferroptosis inducer erastin increased ROS levels in trophoblast cells. The ferroptosis inhibitor Fer-1, the apoptosis inhibitor Z-VAD-FMK, and the necrosis inhibitor Nec-1 failed to prevent erastin-induced ROS elevation. In p53 + / + trophoblasts, erastin-induced ROS elevation was more pronounced than that in p53 − / − and control cells, and angiogenesis was impaired. In pregnant rats, p53 + / + placentas exhibited increased MDA and total iron levels, ferroptosis-like morphological changes in trophoblasts, and reduced CD34 expression. p53 protein expression was negatively correlated with CD34 expression.

Conclusion This study confirmed that trophoblast ferroptosis occurs in the pathological state of PE and that trophoblast are specifically sensitive to ferroptosis. p53 can mediate the SLC7A11/GPX4 signaling pathway to promote ferroptosis of trophoblast cells in the pathogenesis of PE. It is also speculated that increased p53 reactivity may mediate impaired angiogenesis in placental tissues.

Keywords Preeclampsia, Ferroptosis, P53, SLC7 A11/GPX4

†Tingting Liao and Xia Xu contributed equally to this work.

*Correspondence:
Jianying Yan
yanjy2019@fjmu.edu.cn

Background

Preeclampsia (PE) is a multisystem pregnancy-related disorder characterized by maternal hypertension and proteinuria, with a global incidence of 5 to 7%. Because PE may progress to eclampsia (a form of convulsion) due to late-onset, delayed diagnosis and treatment, it is necessary to identify reliable markers for the early diagnosis of PE and develop effective treatment strategies. The disruption of biological processes in placental villous trophoblastic cells leads to various forms of programmed cell death, which is considered to be the key mechanism of PE pathogenesis. The etiology and pathogenesis of preeclampsia are complex and multifactorial, which may be related to an increased inflammatory condition [1], oxidative stress [2], and metabolic dysfunctions [3] at the maternal–fetal interface. This dysregulation contributes to abnormal placental formation and enhanced apoptosis, relating in insufficient placental invasion, vascular remodeling disorders, and impaired microcirculation [4]. Ferroptosis is a unique, non-programmed mode of cell death characterized by the accumulation of iron, lipid hydrogen peroxide and their metabolites in the cytoplasm and by the peroxidation of polyunsaturated fatty acids (PUFAs) in the plasma membrane. Ferroptosis differs from apoptosis and necrosis in morphology, heredity, and biochemistry. It is characterized by decreased depletion of glutathione (GSH) and inactivation of glutathione peroxidase 4 (GPX4) due to increased transport of Fe^{2+} within the cell. When free iron is present, GPX4 can catalyze the reduction of lipid hydrogen peroxide to nonreactive lipid alcohol and prevent the Fenton reaction of lipid hydrogen peroxide [5]. Solute carrier family 7, member 11 (SLC7 A11) can import extracellular cystine and export glutamate to promote GSH biosynthesis and protect cells from oxidative stress (OS) [6]. Oxidative stress, cell damage, and death caused by hypoxia and mitochondrial dysfunction are the main causes of placental damage in preeclampsia patients [7]. Dysfunctional iron metabolism is involved in a variety of physiological and pathological processes, including cancer cell death, neurotoxicity, neurodegenerative diseases, acute renal failure, drug-induced hepatotoxicity, ischemia/reperfusion injury of the liver and heart, and T-cell immunity [8]. Chen et al. reported that ferroptosis can mediate osteogenic and angiogenic dysfunction. Ferroptosis inhibitors can reduce the excessive production of reactive oxygen species (ROS) in human osteoblast-like MG63 cells and human umbilical vein endothelial cells (HUVECs), promoting osteogenesis and angiogenesis [9]. Although placental OS and lipid toxicity are characteristic manifestations of placental dysfunction [10, 11], the possible role of ferroptosis in placental dysfunction remains largely unclear.

The tumor suppressor p53 (TP53) is an evolutionarily conserved protein that plays an important role in regulating cell proliferation, differentiation, death, and metabolism [12]. TP53 is stimulated by a variety of external or internal pressures and is often described as the "guardian of the genome" [13]. Bao et al. reported that CIRC-DMNT1 and p53 are highly expressed in gestational diabetes mellitus (GDM) and PE patients. CIRC-DMNT1 combined with p53 can activate the JAK/STAT pathway to upregulate p-JAK and p-STAT expression. Increased p-JAK and p-STAT inhibit the survival, proliferation, migration, invasion, and cell cycle progression of trophoblast cells. The inhibition of trophoblast cell growth and function contributes to the progression of GDM and PE [14]. p53 regulates cell division, DNA replication, and the cell cycle and plays a key role in the differentiation of various tissues and organs. Under normal circumstances, the p53 protein is turned off during cell stress and excessive division and proliferation, and when cell damage is beyond repair, p53 triggers programmed cell death by activating apoptosis-related genes [14]. Another study confirmed that ferroptosis (iron-dependent nonapoptotic cell death) is another mechanism that contributes to TP53 function, suggesting that TP53 can regulate different types of cell death under different environmental stimuli. p53 can regulate the expression of ferroptosis-related genes in the nucleus and directly control the activity of ferroptosis-related molecules in the cytoplasm. Ferroptosis was enhanced by the inhibition of SLC7 A11 or an increase in spermidine/spermine N1-acetyltransferase expression. Ferroptosis can be inhibited by either directly inhibiting dipeptidyl peptidase-4 (DPP4) activity or inducing CDKN1 A/p21 expression [15].

The p53 tumor suppressor protein and its main negative regulatory factors murine double minute 2 (MDM2) and MDMX oncoprotein constitute the MDM2/MDMX-p53 circuit. It plays a key role in regulating the growth, proliferation, cell cycle progression, apoptosis, senescence, angiogenesis, and immune response of cells [16]. Yang et al. reported that overexpression of the human umbilical vein endothelial cell receptor UNC5B promoted intracellular ROS production, activated the p53 pathway, inhibited cell migration and tubular function, and promoted endothelial cell senescence [17]. Pfaff et al. confirmed through animal experiments that p53 negatively regulates ischemia-induced angiogenesis. Deletion of p53 can upregulate the expression of hypoxia-inducible factor 1α (HIF-1α) and vascular endothelial growth factor (VEGF), which mediate endothelial cell growth and increase limb perfusion, capillary density, and collateral artery development [18]. The characteristics of placental vascular remodeling disorders in PE patients include excessive OS and lipid toxicity, but the possible

role of ferroptosis, especially p53-mediated trophoblastic ferroptosis, in placental dysfunction remains largely unclear. This study aimed to explore the role and mechanism of the p53-mediated SLC7 A11/GPX4 signaling pathway in regulating trophoblast ferroptosis during PE placental angiogenesis to provide new ideas and insights for basic research on PE.

Results

Baseline characteristics

Table 1 shows that the parity ($P=0.725$) and delivery time ($P=0.808$) of pregnant women in the PE group were not significantly different from those in the CTL group. The number of gestational weeks in the PE group was lower than that in the CTL group ($P=0.001$), and age ($P=0.029$), prenatal BMI ($P<0.001$), systolic blood pressure (SP) ($P<0.001$), and diastolic blood pressure (DP) ($P<0.001$) were greater in the PE group than in the CTL group.

Sensitivity of trophoblasts to ferroptosis

The ferroptosis inducers erastin (0, 10, 20, 30, 40, and 50 μM) were added to BeWo and HTR-8/SVneo trophoblast cells for 24 h, and the ROS concentration in each group was detected by flow cytometry. Figure 1A shows that the ROS concentration increased with increasing erastin concentration, i.e., cell mortality increased, indicating that trophoblast cells were sensitive to ferroptosis.

Cultured BeWo and HTR-8/SVneo trophoblast cells were cultured in combination or alone with the ferroptosis inducer erastin, ferroptosis inhibitor Fer-1, apoptosis inhibitor Z-VAD-FMK, and necrosis inhibitor Nec-1. As shown in Fig. 1B, after 24 h of co-culture, the ROS concentrations in the erastin, erastin + Z-VAD-FMK, and erastin + Nec-1 groups were greater than those in the CTL group, Fer-1 and erastin + Fer-1 groups ($P<0.05$). The differences in the ROS concentrations among the erastin group, the erastin + Z-VAD-FMK group, the erastin + Nec-1 group, the CTL group, the Fer-1 group, and the erastin + Fer-1 group were not statistically significant ($P>0.05$). These results indicated that trophoblast cells were specifically sensitive to ferroptosis.

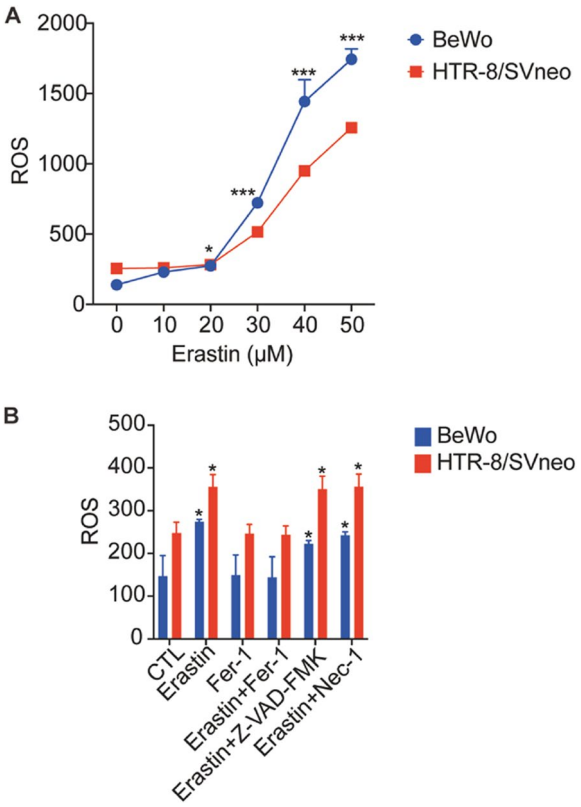

Fig. 1 Sensitivity of trophoblast cells to ferroptosis. **A** Effects of ferroptosis inducer Erastin on ROS concentrations in trophoblasts. With the gradual increase of the ferroptosis inducer Erastin concentration, the mortality rate of trophoblasts increased significantly (P1 < 0.001, P2 < 0.001). Differences among groups were compared by single factor analysis of variance (ANOVA). **B** Effects of ferroptosis inducer Erastin and ferroptosis inhibitor Fer-1 on the concentration of ROS in trophoblasts. * means compared to the CTL group, the Fer-1 group, and the Erastin + Fer-1 group, the mortality rate of BeWo and HTR-8/SVneo cells in the Erastin group, the Erastin + Z-VAD-FMK group, and the Erastin + Nec-1 group increased significantly ($P<0.05$) (biological replicates number: 1). Differences among groups were compared by single factor analysis of variance (ANOVA) the type of post hoc test used LSD

Table 1 Baseline characteristics of the women included in this analysis ($\overline{X} \pm S$)

	PE group ($n=30$)	CTL group ($n=30$)
Age (year)	31.93 ± 5.45*	28.80 ± 5.40
Gestational weeks (week)	35.97 ± 3.34**	38.37 ± 0.96
Parity time	1.43 ± 0.68	1.50 ± 0.78
Delivery time	0.27 ± 0.52	0.30 ± 0.54
Prenatal BMI (kg/m^2)	28.35 ± 4.29***	22.55 ± 3.32
SP (mmHg)	137.90 ± 14.81***	118.93 ± 8.30
DP (mmHg)	91.83 ± 9.37***	76.47 ± 6.28

S Standard deviation, *BMI* Body mass index, *SP* Systolic pressure, *DP* Diastolic pressure

*means compared with the CTL group $P<0.05$

**means compared with the CTL group $P<0.01$

***means compared with the CTL group $P<0.001$. Comparison between two groups was conducted by the independent sample *t*-test

The pathological state of PE is characterized by ferroptosis of trophoblasts

The concentrations of ferroptosis markers (MDA and total iron) in the placental tissues of pregnant women and pregnant rats in the PE and CTL groups were

detected, and the morphological changes in trophoblast cells in placental tissues were observed via transmission electron microscopy. Figure 2A and B show that the concentrations of MDA and total iron in the placental tissue of pregnant women and pregnant rats in the PE group were greater than those in the CTL group. Figure 2C shows slight overall swelling of placental cytotrophoblast cells in pregnant women in the CTL group, no obvious signs of ferroptosis, more organelles, and a continuous basement membrane (BM). The nucleus (N) had an irregular shape, slight local indentation, and a heterochromatin edge set. The mitochondria (M) were slightly swollen, most of the structures were acceptable, cristae were present, the membrane was intact, and the matrix within the membrane of some mitochondria was weakened. The rough endoplasmic reticulum (RER) was enlarged and vacuolated, and the ribosome had degranulated. Figure 2D shows that the placental syncytiotrophoblast cells of pregnant women in the PE group exhibited ferroptosis overall, with abundant microvilli (Mv) around the cell membrane, a uniform distribution of the intracellular matrix, a continuous basement membrane (BM), and local hypertrophy. The nucleus (N) had an irregular shape, was locally concave, had a heterochromatin edge set, and had a visible nucleolus (Nu). The rough endoplasmic reticulum (RER) is characterized by dilatation and surface ribosome degranulation. Figure 2E shows that the placental syncytiotrophoblast cells of pregnant rats in the CTL group exhibited mild to moderate swelling, complete and continuous cell membranes, and sparse microvilli (Mv). The cell matrix became shallow and dissolved locally, and the organelles were moderate in number, concentrated in distribution, and obviously swollen. The intercellular space was fair. The nucleus (N) was approximately elliptical, the double-layer nuclear membrane was clear, the perinuclear space was not significantly widened, and the amount of heterochromatin was slightly increased. The number of mitochondria (M) was moderate, mostly oval, with mild to moderate swelling, and the matrix became shallow and dissolved. The rough endoplasmic reticulum (RER) was less abundant and clearly expanded, and ribosome attachment was visible on the surface. Autophagolysosomes (ASSs) were observed. Figure 2F shows signs of ferroptosis in the placental syncytiotrophoblast cells of pregnant rats in the PE group, moderate swelling, complete and continuous cell membrane, and sparse microvilli (Mv). The electron density of the cell matrix was slightly low, the number of organelles was moderate, and the organelles were scattered and obviously swollen. The intercellular space was fair. The nucleus (N) was approximately elliptical and slightly dented locally, the nuclear membrane was blurred locally, the perinuclear space was slightly widened (black arrow), heterochromatin was increased, and edge sets were set. The number of mitochondria (M) was moderate, some of which were slightly smaller, the electron density of the membrane and matrix was greater, and the ridge was obviously expanded. The rough endoplasmic reticulum (RER) was small in number and obviously enlarged, and the surface ribosome had degranulated. The pathological state of PE was confirmed to involve ferroptosis of trophoblasts.

p53 regulated the SLC7 A11/GPX4 signaling pathway to promote ferroptosis in trophoblast cells

qRT-PCR, WB, and IHC were used to detect the expression levels of p53 and SLC7 A11/GPX4 signaling pathway components in the placental tissues of pregnant women. Figure 3A–E shows that the expression levels of p53 mRNA and protein and the percentage of positive cells in placental tissues of pregnant women in the PE group were greater than those in the CTL group, and the expression levels of SLC7 A11 and GPX4 mRNA and protein and the percentage of positive cells were decreased compared with those in the CTL group.

Further investigation revealed that the protein expression levels of p53 in the placental tissues of pregnant women in the PE and CTL groups were negatively correlated with the protein expression levels of the SLC7 A11/GPX4 signaling pathway and positively correlated with the MDA and total iron concentrations. It is speculated that p53 could regulate the SLC7 A11/GPX4 signaling pathway to promote ferroptosis of trophoblast cells and participate in the pathogenesis of PE (see Table 2 & Fig. 3F–I).

(See figure on next page.)

Fig. 2 Expression levels of ferroptosis markers in placental tissues. **A**,**B** Expression levels of ferroptosis markers (MDA and total iron) in placental tissue from normal and preeclamptic pregnant women (**A**) and pregnant rats **B**. * means compared with the CTL group, it was significantly different in the PE group ($P < 0.05$). *** means compared with the CTL group, it was significantly different in the PE group ($P < 0.001$). **C**,**D** Morphology of placental trophoblasts from normal and preeclamptic pregnant women (magnification 2500). **C** The CTL group, **D** the PE group. **E**,**F** Morphology of placental trophoblasts from normal and preeclamptic pregnant rats (magnification 2500). **E** The CTL group, **F** the PE group. The phenomenon of ferroptosis in the PE group was more serious than that in the CTL group. Comparison between two groups was conducted by the independent sample t-test

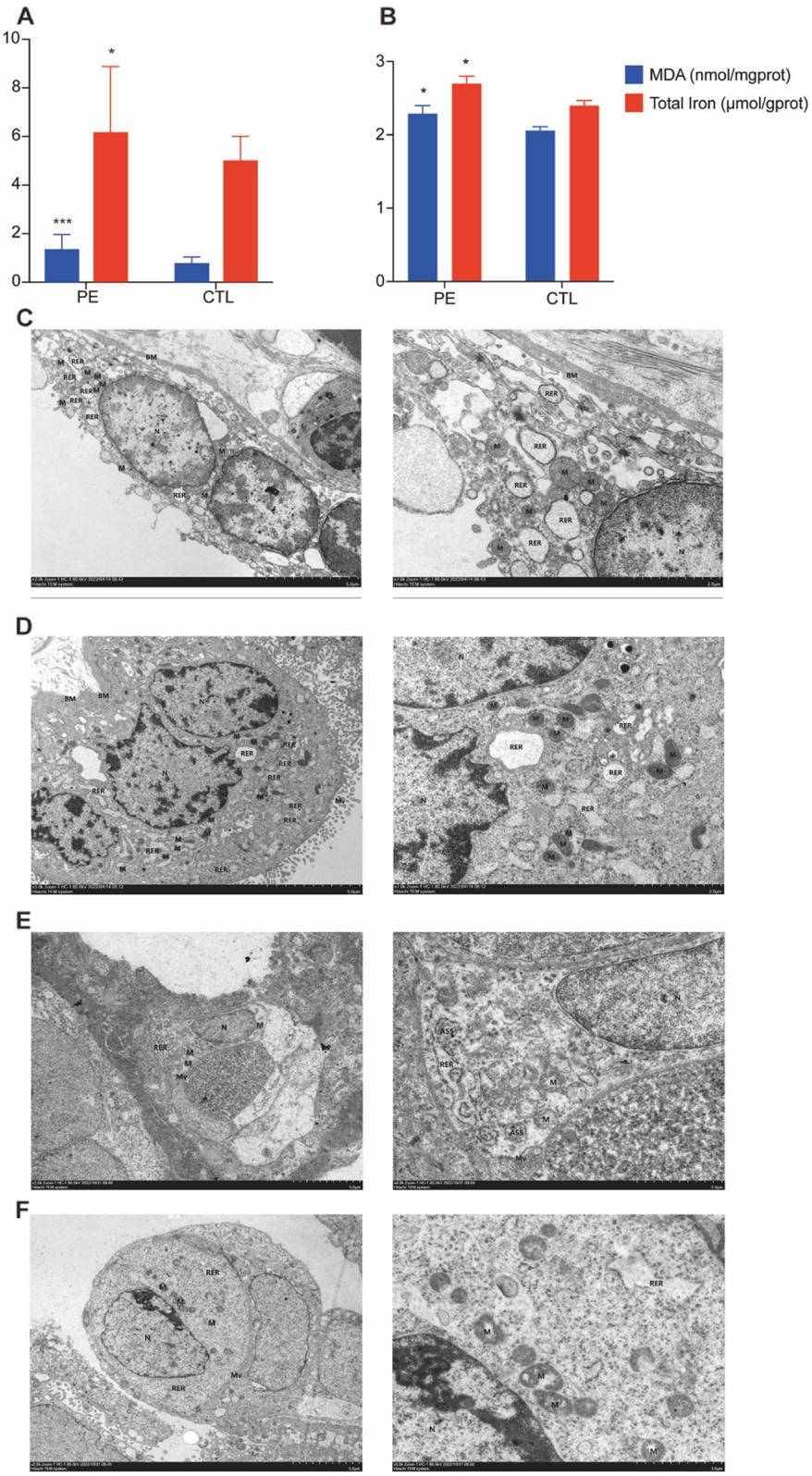

Fig. 2 (See legend on previous page.)

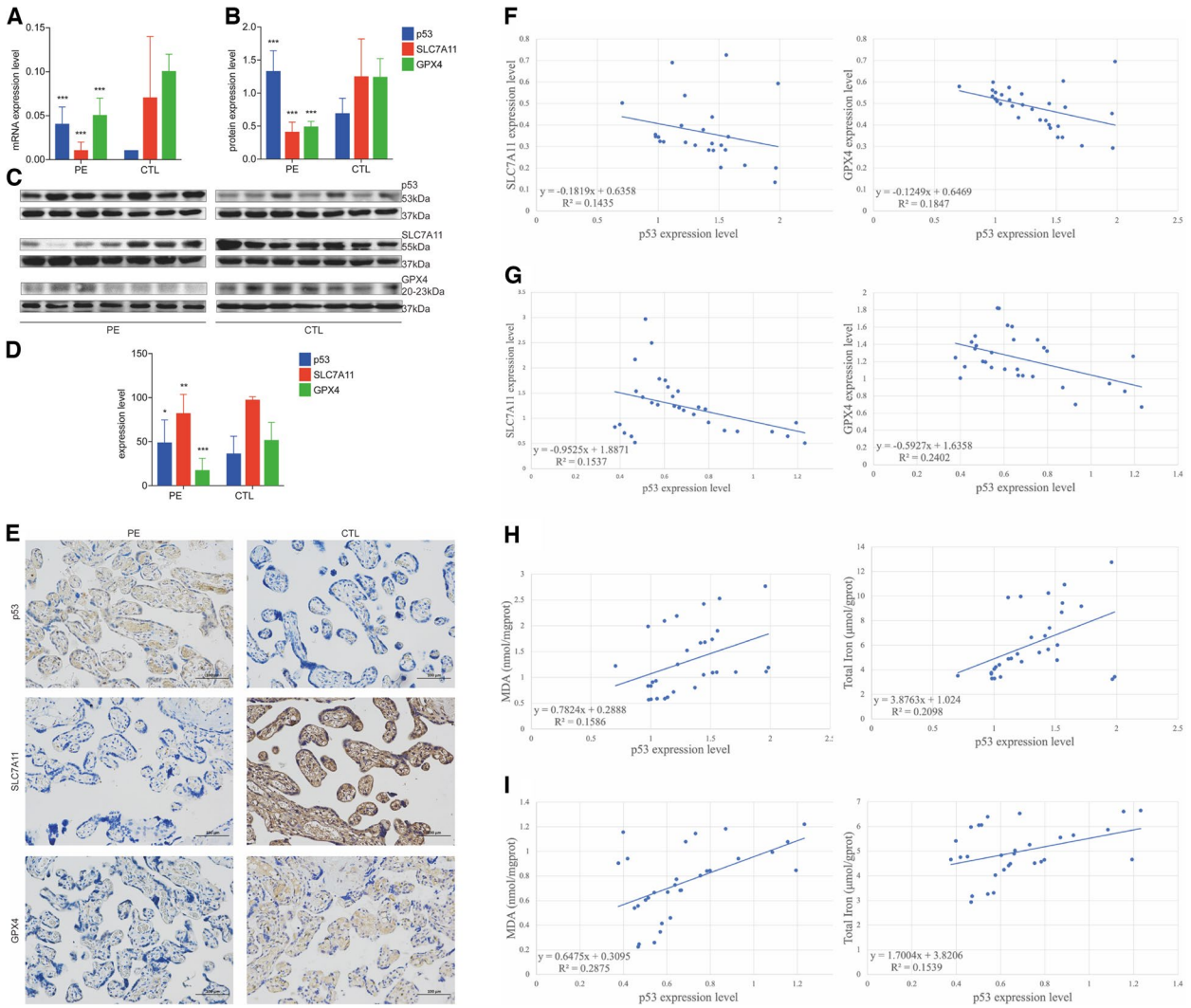

Fig. 3 Expression levels of p53 and SLC7 A11/GPX4 signaling pathway in placental tissues. **A–E** Expression levels of p53 and SLC7 A11/GPX4 signaling pathway in placental tissues. **A** p53 and SLC7 A11/GPX4 signal pathway mRNA expression levels in placental tissue from normal and preeclamptic pregnancies. *** means in reverse transcriptase-polymerase chain reaction (RT-PCR), expression levels of p53 and SLC7 A11/GPX4 signal pathway mRNA were significantly different in the PE group compared with the CTL group ($P < 0.001$). **B**,**C** p53 and SLC7 A11/GPX4 signal pathway protein expression levels in placental tissue from normal and preeclamptic pregnancies. The PE and the control were run in the same blot, incubated separated at the same time, and then co-exposing. *** means in Western blot (WB), expression levels of p53 and SLC7 A11/GPX4 signal pathway protein were significantly different in the PE group compared with the CTL group ($P < 0.001$). **D**,**E** p53 and SLC7 A11/GPX4 signal pathway protein expression levels in placental tissue from normal and preeclamptic pregnancies (in brown). * means in immunohistochemistry (IHC), expression levels of p53 protein in the PE group were higher than the CTL group significantly ($P < 0.05$). ** means in immunohistochemistry (IHC), expression levels of SLC7 A11 protein in the PE group were lower than the CTL group significantly ($P < 0.01$). *** means in immunohistochemistry (IHC), expression levels of GPX4 protein in the PE group were lower than the CTL group significantly ($P < 0.001$). Comparison between two groups was conducted by the independent sample t-test. **F–I** Analyzed correlation between p53 protein expression and SLC7 A11/GPX4 signaling pathway protein expression, MDA and total iron concentration in placenta tissues of the two groups. F,H The expression level of p53 protein in the PE group was negatively correlated with the expression levels of the SLC7 A11/GPX4 signaling pathway protein (P1 = 0.039, P2 = 0.018), and positively correlated with the concentrations of MDA ($P = 0.029$) and total iron ($P = 0.011$). **G**,**I** The expression level of p53 protein in the CTL group was negatively correlated with the expression levels of the SLC7 A11/GPX4 signaling pathway protein (P1 = 0.032, P2 = 0.006), and positively correlated with the concentrations of MDA ($P = 0.002$) and total iron ($P = 0.032$)

Based on the results of tissue experiments, to explore whether p53 can regulate the SLC7 A11/GPX4 signaling pathway to promote ferroptosis in trophoblast cells, we constructed trophoblast cell lines with different p53 expression levels. After coculture of the p53 inducer Nutlin-3 with trophoblast cells for 72 h and the p53 inhibitor

Table 2 Analyzed correlation between p53 protein expression and SLC7 A11/GPX4 signaling pathway protein expression, MDA, and total iron concentration in placenta tissues of the two groups (*r* value)

Group	SLC7 A11	GPX4	MDA	Total iron
PE group ($n=30$)	-0.38^{*}	-0.43^{*}	0.40^{*}	0.46^{*}
CTL group ($n=30$)	-0.39^{*}	-0.49^{**}	0.54^{**}	0.39^{*}

MDA Malondialdehyde, *SLC7 A11* Solute carrier family 7, member 11, *GPX4* Glutathione peroxidase 4

* compared with the p53 group $P<0.05$

** compared with the p53 group $P<0.01$

MG-132 with trophoblast cells for 48 h, the expression levels of p53 downstream signal molecules in BeWo and HTR-8/SVneo cells were detected by CUT&Tag technology and the mRNA and protein expression levels of p53 and SLC7 A11/GPX4 signaling pathway components in BeWo and HTR-8/SVneo cells were measured qRT-PCR and WB. According to the rpkm values of all peaks in each sample, the correlation coefficients of intra-group and inter-group samples were calculated. Figure 4A1, A2 show that the expression pattern was highly similar among samples. Figure 4B1, B2 show that the abundance of SLC7 A11 peaks in the p53 gene promoter region in the p53 +/+ group was significantly lower than that in the p53 −/− and the CTL groups. The abundance of SLC7 A11 peaks in p53 gene promoter region in the p53 −/− group was significantly higher than that in p53 +/+ and CTL groups. As shown in Fig. 4C1–F, the p53 mRNA and protein levels in the p53 +/+ group were greater than those in the p53 −/− group and the CTL group, while the p53 mRNA and protein levels in the p53 −/− group were less than those in the p53 +/+ group and the CTL group. The mRNA and protein expression levels of SLC7 A11 and GPX4 in the p53 +/+ group were lower than those in the p53 −/− group and CTL group, and the mRNA and protein expression levels of SLC7 A11 and GPX4 in the p53 −/− group were greater than those in the p53 +/+ group and CTL group.

After trophoblast cells with different p53 expression levels were successfully generated, trophoblast cells were cultured with the ferroptosis inducer erastin (20 μM) for 24, 48 or 72 h to explore whether different p53 expression levels can regulate the SLC7 A11/GPX4 signaling pathway and affect the sensitivity of trophoblast cells to ferroptosis. Figure 4G,I shows that the ROS concentrations in the p53 +/+ group, the p53 −/− group and the CTL group increased with increasing culture time. Figure 4H,J shows that during the three incubation periods, the ROS concentrations in the cells in the p53 +/+ group were greater than those in the p53 −/− group and the CTL group, and the ROS concentrations in the cells in the p53 −/− group were less than those in the p53 +/+ group and the CTL group, which proved that different p53 expression levels could affect the sensitivity of trophoblast cell lines to ferroptosis.

To further explore whether p53 affects trophoblast sensitivity to ferroptosis by regulating the SLC7 A11/GPX4 signaling pathway, we constructed a trophoblast cell line with SLC7 A11 inhibitory expression (SLC7 A11 −/−) (Fig. 4K–M) and cocultured it with the ferroptosis inducer erastin (20 μM)for 24 h. Figure 4N shows that the ROS concentration in the SLC7 A11 −/− group was greater than that in the CTL group ($P<0.01$), which confirmed that p53 could specifically regulate the SLC7 A11/GPX4 signaling pathway and affect the sensitivity of trophoblast cells to ferroptosis.

The above conclusions were verified in animal experiments. L-NAME was used to construct a PE rat model, and the p53 inducer Nutlin-3 and p53 inhibitor MG-132 were used to construct PE rat models of p53 overexpression (p53 +/+) and inhibition (p53 −/−), after which

(See figure on next page.)

Fig. 4 Erastin affects the concentrations of ROS in trophoblast cells. A1–B2 Downstream signaling molecules of p53 in trophoblast cells with different expression levels of p53. C1–F Expression levels of p53 and SLC7 A11/GPX4 signaling pathway in trophoblasts with different expression levels of p53. C1,C2 Expression levels of p53 and SLC7 A11/GPX4 signaling pathway mRNA in trophoblasts with different expression levels of p53. D1–F Expression levels of p53 and SLC7 A11/GPX4 signaling pathway proteins in trophoblasts with different expression levels of p53. * means expression levels of p53 and SLC7 A11/GPX4 signal pathway were significantly different ($P<0.05$). ** means expression levels of p53 and SLC7 A11/GPX4 signal pathway were significantly different ($P<0.01$). *** means expression levels of p53 and SLC7 A11/GPX4 signal pathway were significantly different ($P<0.001$). **G–J** Erastin affected the concentrations of ROS in trophoblast cells with different expression levels of p53. **G**,**H** Erastin affected the concentrations of ROS in BeWo cells with different expression levels of p53. I,J Erastin affected the concentrations of ROS in HTR-8/SVneo cells with different expression levels of p53. *** means the concentrations of ROS significantly different ($P<0.001$). K–N Erastin affected the concentrations of ROS in trophoblast cells with different expression levels of SLC7 A11. **K–M** Expression levels of p53 and SLC7 A11/GPX4 signaling pathway proteins in trophoblasts with different expression levels of SLC7 A11. **N** Erastin affected the concentrations of ROS in BeWo and HTR-8/SVneo cells with different expression levels of SLC7 A11. * means expression levels of p53 and SLC7 A11/GPX4 signal pathway were significantly different ($P<0.05$). ** means expression levels of p53 and SLC7 A11/GPX4 signal pathway were significantly different ($P<0.01$). *** means expression levels of p53 and SLC7 A11/GPX4 signal pathway were significantly different ($P<0.001$). ** means the concentrations of ROS significantly different ($P<0.01$) (biological replicates number: 2). Differences among groups were compared by single factor analysis of variance (ANOVA) the type of post hoc test used LSD

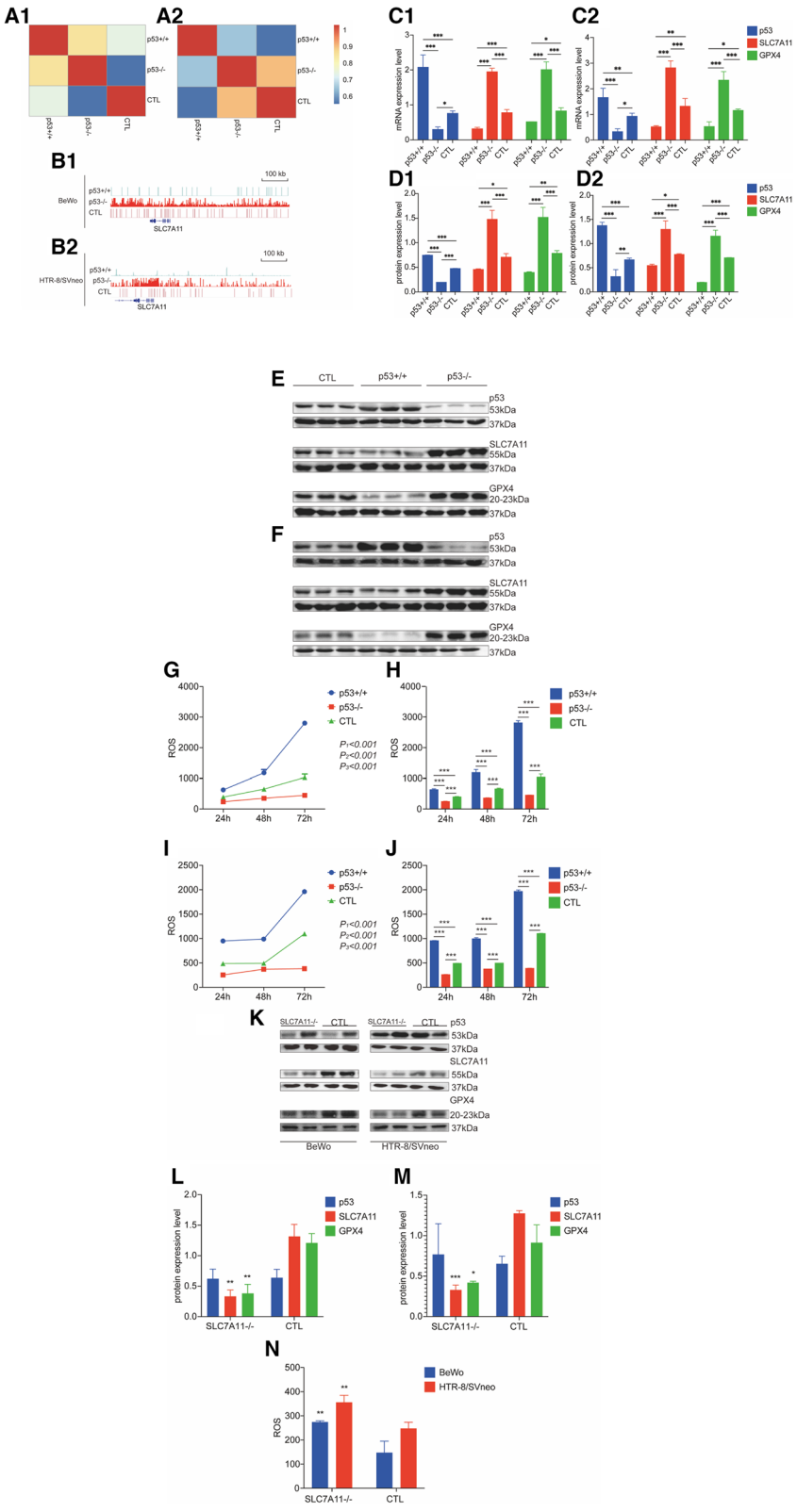

Fig. 4 (See legend on previous page.)

the general condition of each group of rats was evaluated. Table 3 shows that the body weights of pregnant rats in the p53 +/+ group were lower than those in the p53 −/− group and the CTL group. The body weights of fetal rats in the p53 +/+ group were lower than those in the p53 −/− group, the PE group, and the CTL group. The stillbirth rate of pregnant rats in the p53 +/+ group was greater than that in the p53 −/− group and the CTL group. There was no significant difference in the number of fetal rats among all groups.

The levels of SP and urinary protein before and after modeling were compared in all groups. Figure 5A–D shows that there was no significant difference in SP or urinary protein concentration between the CTL and p53 −/− groups before and after modeling, while the levels of SP and urinary protein concentration in the PE and p53 +/+ groups increased compared with those before modeling. After modeling, the SP and urine protein concentrations in the p53 +/+ group were greater than those in the p53 −/− group, the PE group and the CTL group, while those in the p53 −/− group were less than those in the p53 +/+ group and the PE group, and the difference was not statistically significant compared with that in the CTL group.

The mRNA and protein expression levels of p53 and genes involved in the SLC7 A11/GPX4 signaling pathway in the placental tissues of pregnant rats were measured by qRT-PCR, WB, and immunofluorescence. Figure 5E–L shows that the expression levels of p53 mRNA and protein in pregnant rats in the p53 +/+ group were greater than those in the p53 −/− group and the PE group, and the expression levels of p53 mRNA and protein in pregnant rats in the p53 −/− group were less than those in the p53 +/+ group and the PE group. The expression levels of SLC7 A11 and GPX4 mRNA and protein in pregnant rats in the p53 +/+ group were lower than those in the p53 −/− group and the PE group, while the expression levels of SLC7 A11 and GPX4 mRNA and protein in pregnant rats in the p53 −/− group were greater than those in the p53 +/+ group and the PE group, indicating that PE rat models with different expression levels of p53 were successfully constructed. p53 is an upstream signaling molecule that regulates the expression level of the SLC7 A11/GPX4 signaling pathway.

To further explore whether p53 can regulate the SLC7 A11/GPX4 signaling pathway to promote ferroptosis in trophoblast cells, we detected the concentrations of ferroptosis markers (MDA and total iron) in the placental tissue of PE model rats with different p53 expression levels and observed morphological changes in placental trophoblast tissues via transmission electron microscopy. Figure 6A,B shows that the concentrations of MDA and total iron in pregnant rats in the p53 +/+ group were greater than those in the p53 −/− group, the PE group and the CTL group, while the concentrations of MDA and total iron in pregnant rats in the p53 −/− group were less than those in the p53 +/+ group, the PE group, and the CTL group. Figure 6C shows that the placental cystotrophoblast cells of pregnant rats in the p53 +/+ group exhibited ferroptosis overall, a slightly widened cell space, abundant microvilli (Mv) around the cell membrane, slight thickening and rounding of some organelles, a slightly uneven distribution of organelles, and a continuous basal membrane (BM). The nucleus (N) is approximately oval, with a slightly dented heterochromatin edge set. The number of mitochondria (M) increased significantly with increased membrane density, high electron density, iron deposition, and slight ridge expansion. The rough endoplasmic reticulum (RER) was enlarged and vacuolated, and the ribosome had degranulated. Figure 6D shows that the syncytiotrophoblast cells of the placenta were moderately or severely swollen, the cell membrane was not damaged, and the microvilli (Mv) were sparse. The distribution of the cell matrix was slightly heterogeneous, the number of organelles was moderate, and the organelles were scattered and swollen.

Table 3 Comparing general conditions of PE rats with different expression levels of p53 ($\bar{X} \pm S$)

	Body weight of pregnant rats (g)	Body weight of fetal rats (g)	Number of fetal rats	Stillbirth rate of pregnant rats (%)
CTL group ($n = 8$)	353.69 ± 45.23	1.26 ± 0.56	11.75 ± 3.92	6.63 ± 8.36
PE group ($n = 8$)	313.13 ± 30.35*	1.50 ± 1.09*	12.13 ± 2.10	30.57 ± 23.64**
p53 +/+ group ($n = 8$)	294.38 ± 24.35***	0.45 ± 0.23***	13.63 ± 3.58	32.12 ± 9.15**
p53 −/− group ($n = 8$)	333.38 ± 26.74	1.25 ± 0.14	13.63 ± 1.41	10.18 ± 14.34

S Standard deviation. Differences among groups were compared by single factor analysis of variance (ANOVA) the type of post hoc test used LSD

*means compared with the CTL group $P < 0.05$

**means compared with the CTL group $P < 0.01$

***means compared with the CTL group $P < 0.001$

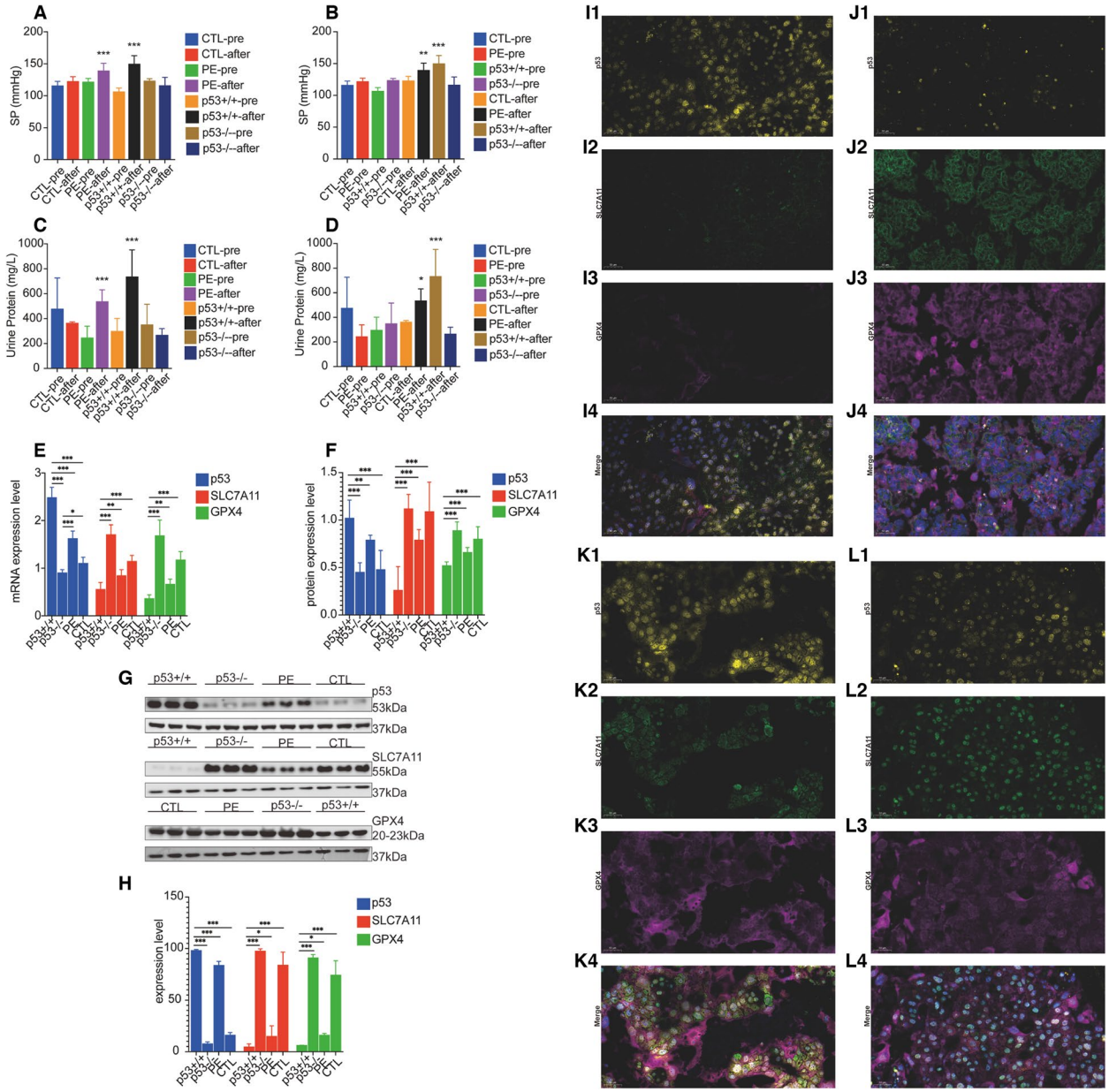

Fig. 5 Expression levels of p53 and SLC7 A11/GPX4 signaling pathway in placental tissues of PE rats with different expression levels of p53. A–D Comparing general conditions of PE rats with different expression levels of p53. * means it was significantly different ($P < 0.05$). ** means it was significantly different ($P < 0.01$). *** means it was significantly different ($P < 0.001$). E–L Expression levels of p53 and SLC7 A11/GPX4 signaling pathway in placental tissues of PE rats with different expression levels of p53. E p53 and SLC7 A11/GPX4 signal pathway mRNA expression levels in placental tissues from normal and preeclamptic pregnant rats. F–L p53 and SLC7 A11/GPX4 signal pathway protein expression levels in placental tissues from normal and preeclamptic pregnant rats. * means expression levels of p53 and SLC7 A11/GPX4 signaling pathway were significantly different compared with the p53 +/+ group ($P < 0.05$). ** means expression levels of p53 and SLC7 A11/GPX4 signaling pathway were significantly different compared with the p53 +/+ group ($P < 0.01$). *** means expression levels of p53 and SLC7 A11/GPX4 signaling pathway were significantly different compared with the p53 +/+ group ($P < 0.001$). Differences among groups were compared by single factor analysis of variance (ANOVA) the type of post hoc test used LSD

The intercellular space was acceptable. The nucleus (N) was approximately oval and partially depressed, the nuclear membrane was clear, the perinuclear space was slightly widened (black arrows), and the chromatin was evenly distributed. The mitochondria (M) were moderate in number, small in volume, without obvious swelling, with an intact membrane and a deep matrix density. The rough endoplasmic reticulum (RER) was dilated,

degranulated, and vacuolated. These findings indicate that the ferroptosis levels of trophoblast cells in PE model rats with different p53 expression levels are different.

Further exploration revealed that the p53 protein expression levels in the placental tissue of the p53 +/+ group, the p53 −/− group, the PE group, and the CTL group were negatively correlated with the protein expression levels of the SLC7 A11/GPX4 signaling pathway and positively correlated with the MDA and total iron concentrations. In summary, p53 can regulate the SLC7 A11/GPX4 signaling pathway to promote trophoblast ferroptosis and participate in the pathogenesis of PE (see Table 4 and Fig. 6E–H).

Increased p53 reactivity may mediate PE placental angiogenesis disorder

To explore the specific mechanism by which p53 regulates the SLC7 A11/GPX4 signaling pathway to promote ferroptosis in trophoblast cells and participate in the pathogenesis of PE, we detected the expression of factors related to angiogenesis in pregnant placental tissues. Figure 7A shows that the protein expression level of VEGFR1 in the placental tissue of pregnant women in the PE group was greater than that in the CTL group, while the protein expression levels of VEGFA and PLGF were lower in the PE group than in the CTL group.

Table 5 and Fig. 7B–G show that the protein expression levels of p53 in the placental tissues of pregnant women in the PE and CTL groups were positively correlated with VEGFR1 and negatively correlated with VEGFA and PLGF, suggesting that p53 may mediate the SLC7 A11/GPX4 signaling pathway to regulate trophoblast ferroptosis, leading to angiogenesis disorders in placental tissue and participating in the pathogenesis of PE.

To explore whether different p53 expression levels affect the level of angiogenesis in vitro, HUVECs were cocultured with the p53 inducer or inhibitor for 24 h. Figure 7H–K shows that the level of angiogenesis in the p53 +/+ group was lower than that in the p53 −/− group and the CTL group, and there was no significant difference in the level of angiogenesis between the p53 −/− group and the CTL group. It has been confirmed that increased p53 expression can mediate angiogenesis disorders.

WB and IHC were used to detect the expression levels of the angiogenesis marker CD34 in placental tissues from PE model rats with different p53 expression levels. Figure 7L–R shows that the protein expression levels of CD34 and the percentage of CD34-positive cells in the p53 +/+ group were lower than those in the p53 −/− group and the PE group. The expression levels of CD34 protein and the percentage of CD34-positive cells in the p53 −/− group were greater than those in the p53 +/+ group and the PE group.

To explore the correlation between the expression levels of p53 protein in the placentas of PE model rats with different p53 expression levels and the expression levels of angiogenesis-related factors. Figure 7S–V shows that the protein expression levels of p53 in the placentas of pregnant rats in the p53 +/+, p53 −/−, PE, and CTL groups were negatively correlated with the protein expression level of CD34. It has also been confirmed that p53 overexpression may mediate angiogenesis disorders in placental tissue. Taken together, these results indicate that p53 can mediate the SLC7 A11/GPX4 signaling pathway to regulate trophoblast ferroptosis, which may lead to placental tissue angiogenesis disorders and participate in the pathogenesis of PE.

Discussion

Preeclampsia is a pregnancy syndrome characterized by high blood pressure and proteinuria after 20 weeks of gestation [20]. Recent studies have shown that all stages of PE involve incomplete spiral artery transformation and impaired placental development [21], resulting in placental hypoperfusion, ischemia, and hypoxia; triggering inflammation during abnormal placental formation; promoting ROS release in the cell membrane, endoplasmic reticulum, and mitochondria; and damaging proteins and DNA [22, 23]. Abnormal placental formation associated with inadequate invasion of the placenta, vascular remodeling disorders, and impaired microcirculation in PE is associated with a variety of types of programmed

(See figure on next page.)

Fig. 6 Expression levels of ferroptosis markers in placental tissues of PE rats with different expression levels of p53. **A** Concentrations of MDA in placental tissues of PE rats with different expression levels of p53. *** means concentrations of MDA were significantly different ($P < 0.001$). **B** Total iron concentrations in placental tissues of PE rats with different expression levels of p53. *** means concentrations of total iron were significantly different ($P < 0.001$). Differences among groups were compared by single-factor analysis of variance (ANOVA), the type of post hoc test used LSD. **C,D** Morphological observation of placental trophoblasts in PE rats with different expression levels of p53. C The p53 +/+ group, D the p53 −/− group. The phenomenon of ferroptosis in the p53 +/+ group was more serious than that in the p53 −/− group. **E–H** Analyzed the correlation between p53 protein expression and SLC7 A11/GPX4 signaling pathway protein expression, MDA, and total iron concentrations in PE rats with different expression levels of p53. E1,E2,F1,F2,G1,G2,H1,H2 The expression level of p53 protein was positively correlated with the concentrations of MDA and total iron. E3,E4,F3,F4,G3,G4,H3,H4 The expression level of p53 protein was negatively correlated with the expression levels of the SLC7 A11/GPX4 signaling pathway protein

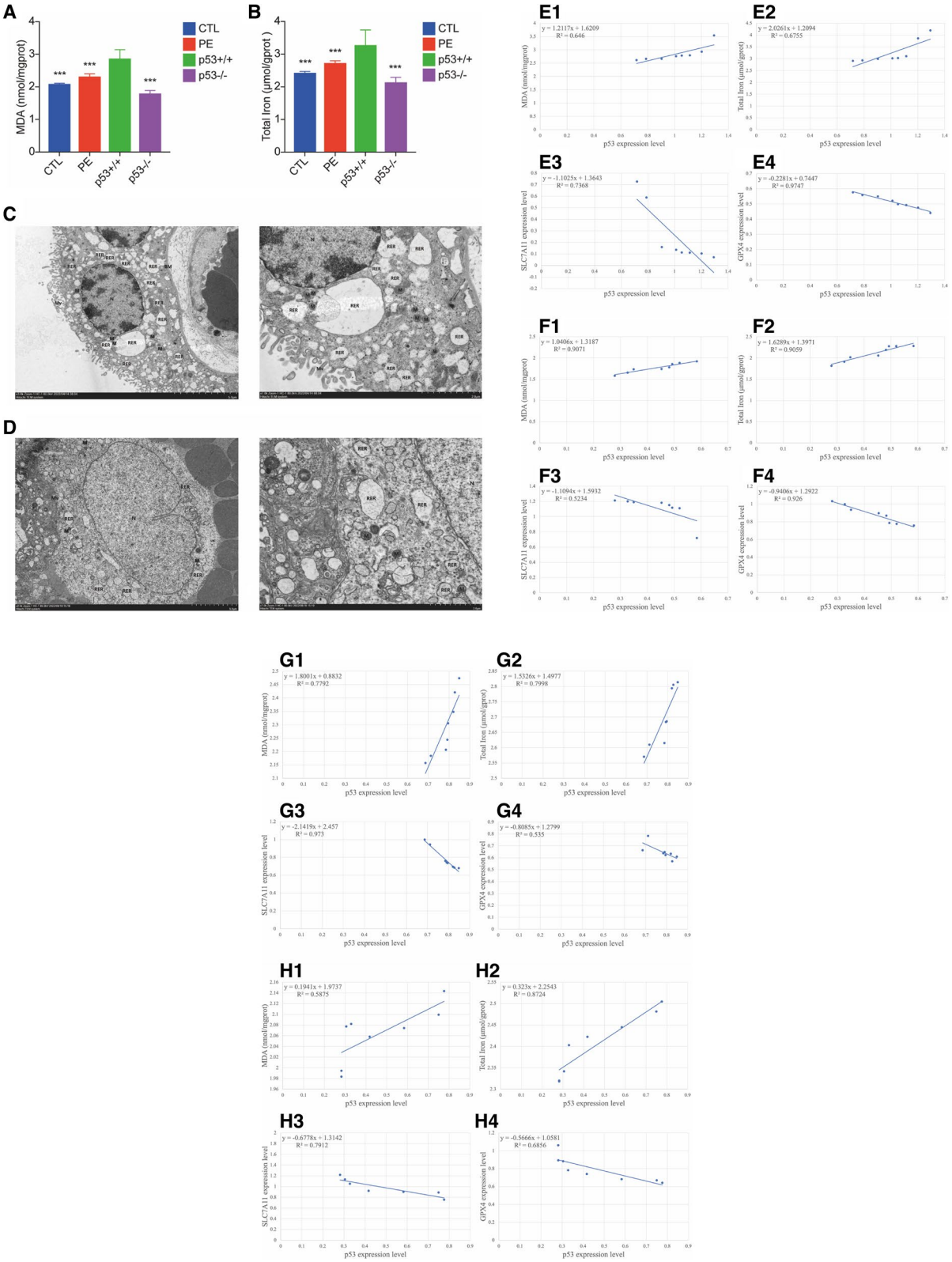

Fig. 6 (See legend on previous page.)

Table 4 Analyzed the correlation between p53 protein expression and SLC7 A11/GPX4 signaling pathway protein expression, MDA, and total iron concentration in PE rats with different expression levels of p53 (*r* value)

Group ($n=8$)	MDA	Total iron	SLC7 A11	GPX4
p53 +/+	0.804*	0.822*	− 0.858**	− 0.987***
p53 −/−	0.952***	0.952***	− 0.723*	− 0.962***
PE	0.883**	0.894**	− 0.986***	− 0.731*
CTL	0.767*	0.934***	− 0.890**	− 0.828*

MDA Malondialdehyde, *SLC7 A11* Solute carrier family 7, member 11, *GPX4* Glutathione peroxidase 4

* compared with the p53 protein expression level $P<0.05$.

** compared with the p53 protein expression level $P<0.01$.

*** compared with the p53 protein expression level $P<0.001$.

cell death, which is considered to be the key mechanism of PE pathogenesis [4]. Zhang et al. found that upregulated miR-30b-5p in the PE rat model could inhibit the expression of SLC7 A11 and FPN1, resulting in decreased GSH and increased unstable Fe^{2+}, which played a key role in trophoblast ferroptosis. Inhibition of miR-30b-5p expression and supplementation with ferroptosis inhibitor can alleviate the symptoms of PE in this rat model, making miR-30b-5p a potential therapeutic target for PE [24]. Our previous study found that Nox2 may trigger ferroptosis in trophoblast cells through STAT3/GPX4 pathway, subsequently leading to regulation of mitochondrial respiration, transition of glycolysis, and inhibition of placental angiogenesis. Therefore, targeted inhibition of Nox2 is expected to become a new therapeutic target for PE [25], and it is found that DJ-1 can mediate trophoblast ferroptosis by regulating the Nrf2/GPX4 signaling pathway and play a protective role in the pathogenesis of PE [26]. This study revealed that p53 could mediate the SLC7 A11/GPX4 signaling pathway to promote ferroptosis of trophoblast cells in the pathogenesis of PE. It is also speculated that increased p53 reactivity may mediate impaired angiogenesis in placental tissues. Therefore, targeted inhibition of p53 is expected to become a new therapeutic target for PE.

Ferroptosis, a newly identified type of regulatory non-apoptotic cell death induced by metabolic stress, is caused by iron-dependent cystine depletion and excessive production of ROS, especially lipide peroxide (LPO) [27]. Plasma membrane phospholipid peroxidation and lipid ROS accumulation mediated by different pathways are the key factors that induce ferroptosis in cells [28] and are also the basis for mediating the complex pathogenesis of PE. The ferroptosis-associated environment is associated with placental physiology and trophoblast damage. These environments include ischemia-hypoxia-reperfusion during placental development, pathological changes in physiological uterine contractions or superficial placental perfusion, trophoblastic iron enrichment, evidence of lipotoxicity during the pathophysiology of major placenta-related diseases such as PE, fetal growth restriction, and preterm birth, and decreased GSH redox capacity and lipid peroxidation repair capacity during placental injury [29]. In this study, by detecting the ROS concentration in trophoblast cells co-cultured with the ferroptosis inducer erastin, ferroptosis inhibitor ferrostatin-1 (Fer-1), apoptosis inhibitor Z-VAD-FMK and necrosis inhibitor necrostatin-1 (Nec-1) and the concentrations of ferroptosis markers in the placental tissue of pregnant women with PE and pregnant rats, we confirmed that trophoblast cells are specifically sensitive to ferroptosis and that ferroptosis occurs in the pathological state of PE. However, due to the differences in the duration and severity of preeclampsia, the data of total placental iron concentration in the preeclampsia group were relatively wide. In the process of specimen collection in subsequent experiments, attention should be paid

(See figure on next page.)

Fig. 7 p53 reactive increase may mediate PE placental angiogenesis disorder. **A** Expression levels of angiogenesis related factors in placental tissues. *** means compared with the CTL group, angiogenesis related factors were significantly different in the PE group ($P<0.001$). Comparison between two groups was conducted by the independent sample t-test. **B–G** Analyzed correlation between p53 protein expression levels and the protein expression levels of angiogenesis-related factors in placenta tissues of the two groups. **B,D,F** The expression levels of p53 protein in the PE group were positively correlated with the expression levels of VEGFR1 protein ($P<0.001$), and negatively correlated with the expression levels of VEGFA ($P=0.003$) and PLGF protein ($P=0.020$). **C,E,G** The expression levels of p53 protein in the CTL group were positively correlated with the expression levels of VEGFR1 protein ($P=0.009$), and negatively correlated with the expression levels of VEGFA ($P<0.001$) and PLGF protein ($P<0.001$). H–K Effect of different expression levels of p53 on angiogenesis. H The p53 +/+ group. I The p53 −/− group. **J** The CTL group. * means the capacities of angiogenesis significantly different ($P<0.05$) (biological replicates number: 4). **L–R** CD34 protein expression levels in placental tissues from PE rats with different expression levels of p53. * means expression levels of CD34 protein were significantly different compared with the p53 +/+ group ($P<0.05$). *** means expression levels of CD34 protein were significantly different compared with the p53 +/+ group ($P<0.001$). Differences among groups were compared by single-factor analysis of variance (ANOVA), the type of post hoc test used LSD. **S–V** Analyzed the correlation between p53 protein expression levels and angiogenesis-related factors protein expression levels in placenta of PE rats with different expression levels of p53. S the p53 +/+ group, T the p53 −/− group, U the PE group, V the CTL group

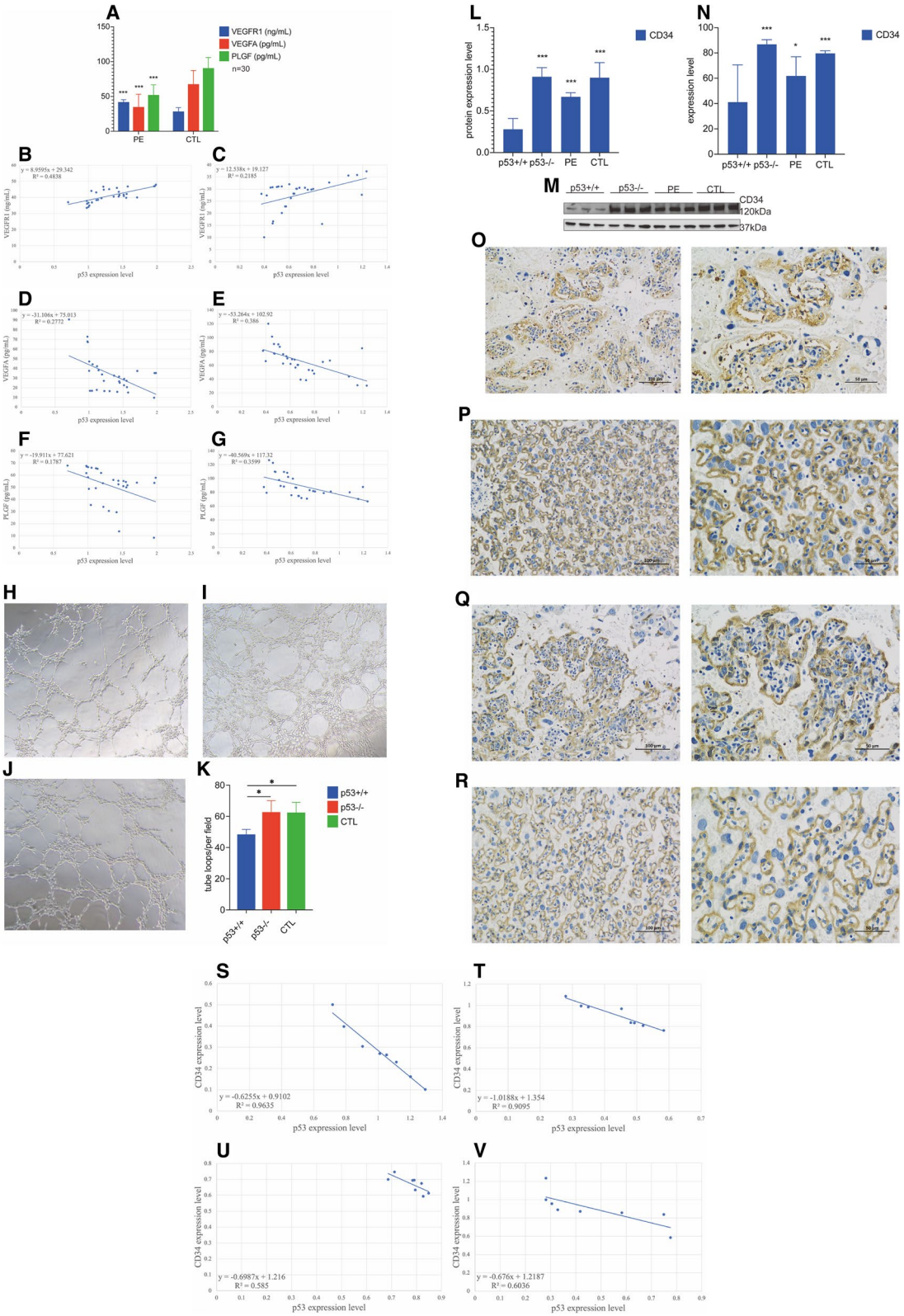

Fig. 7 (See legend on previous page.)

Table 5 Analyzed correlation between p53 protein expression and angiogenesis-related factors protein expression in placenta tissues of the two groups (*r* value)

Group	VEGFR1	VEGFA	PLGF
PE group ($n=30$)	0.696^{***}	-0.526^{**}	-0.423^{*}
CTL group ($n=30$)	0.467^{**}	-0.621^{***}	-0.600^{***}

VEGFR1 Vascular endothelial growth factor receptor 1, *VEGFA* Vascular endothelial growth factor A, *PLGF* Placental growth factor

* compared with the p53 group $P<0.05$

** compared with the p53 group $P<0.01$

*** compared with the p53 group $P<0.001$

to the subdivision of preeclampsia group into early-onset preeclampsia group and late-onset preeclampsia group. Yang et al. reported that there are 20 different ferroptosis-related gene (FRG) subtypes in early-onset preeclampsia (EOPE) and that there are only three FRG subtypes in late-onset preeclampsia (LOPE). Functional enrichment analysis revealed that the differentially expressed FRGs were involved mainly in the pathogenesis of EOPE and were enriched in pathways related to hypoxia and iron metabolism, such as response to hypoxia, regulation of iron homeostasis, and iron ion binding. Protein–protein interaction (PPI) network analysis and qRT-PCR were used to validate the results, which confirmed that ferritin heavy 1 (FTH1), HIF-1α, ferritin 1 (FT1), mitogen-activated protein kinase 8 (MAPK8), and lipid drop-coated protein 2 (PLIN2) were five FRGs, indicating that ferroptosis may be involved in the pathogenesis of PE, especially EOPE [30]. By establishing a PE rat model, Zhang et al. found that compared with those in the control group, the concentrations of MDA and total Fe^{2+} in the placental tissues of the PE group increased, while the GSH content and GPX activity decreased [24], suggesting the occurrence of trophoblast cells ferroptosis in the pathological state of PE, which was consistent with the results of this study.

High mutation of TP53 in cancer cells can abolish the function of typical wild-type p53 to promote cancer development, including by mediating cancer cell proliferation, migration, invasion, initiation, metabolic reprogramming, angiogenesis, and drug resistance [31]. Ferroptosis is a newly discovered form of regulatory cell death. Unlike apoptosis or necrosis, ferroptosis is independent of caspase and receptor interacting protein kinase 1 (RIPK1) activity. Iron-dependent lipid peroxidation mediates cell death [32]. p53 can be recruited to the promoter region of SLC7 A11 to block transcription. SLC7 A11 encodes a component of the cysteine/glutamate antiporter (system Xc-) complex, which is responsible for transporting cysteine, the material for GSH synthesis, into the cell through the heterodimerization of SLC-3 A2 and −7A11 disulfide bonds. Upregulation of p53 can reduce system Xc- activity and GSH production and induce ROS and lipid ROS accumulation to mediate ferroptosis [33]. In this study, trophoblast cells with different p53 expression levels were generated, and the correlations between p53 protein expression levels and SLC7 A11/GPX4 signaling pathway and ferroptosis marker concentrations were analyzed. p53 was confirmed to regulate the SLC7 A11/GPX4 signaling pathway to promote ferroptosis in trophoblast cells. p53 can mediate ferroptosis in different tissues and cells. Guan et al. reported that Tan IIA could upregulate the expression of p53 and inhibit the activity of its target gene SLC7 A11 in BGC-823 and NCI-H87 gastric cancer cells at the mRNA and protein levels, reduce intracellular cysteine and GSH levels, and increase ROS levels. Moreover, p53 gene knockout or the ferroptosis inhibitor Fer-1 can alleviate Tan IIA-induced lipid peroxidation and ferroptosis, indicating that Tan IIA can inhibit gastric cancer proliferation by regulating p53-SLC7 A11 to mediate ferroptosis [34]. Ma et al. established a myocardial ischemia–reperfusion (MI/R) injury model in rats by ligating the left anterior descending coronary artery. They found that the expression levels of p53 increased after 3 h of perfusion and further increased after 24 h of perfusion. Moreover, ROS generation, lipid peroxidation, and Fe^{2+} accumulation increased, while the inhibition of p53 expression had the opposite effect, indicating that p53 could induce ferroptosis in cardiomyocytes by promoting iron accumulation. WB and chromatin immunoprecipitation (ChIP) analyses revealed that p53 overexpression can target and negatively regulate biological activity by binding to the SLC7 A11 promoter [35], indicating that p53 can mediate ferroptosis through multiple pathways at the same time. The role of p53 in regulating ferroptosis varies with the environment and cell type.

The transcription factor p53 plays a gatekeeper role in regulating the expression of numerous genes to maintain normal cell function. An increase in p53 plays a regulatory role by inhibiting angiogenesis, promoting programmed cell death, regulating metabolism, and arresting the cell cycle [36]. As a major transcription factor, the p53 protein is present at very low concentrations in normal cells. When cells are subjected to stress or injury, MDM2 activates p53 through proteasome ubiquitination, inhibits cell proliferation, or mediates apoptosis. Studies have shown that hypoxia and OS during PE pregnancy can stimulate p53 expression, induce trophoblast apoptosis, and inhibit endothelial cell proliferation,

leading to cell apoptosis and excessive autophagy at the level of multiple cell dysfunctions [37]. In this study, we detected the expression levels of angiogenic factors in the placental tissues of pregnant women and pregnant rats, analyzed the correlations between p53 protein expression levels and angiogenic factors, and explored whether the expression levels of p53 and the SLC7 A11/GPX4 signaling pathway affect angiogenesis in vitro. It is speculated that increased p53 reactivity may mediate impaired angiogenesis in placental tissues. Lee et al. reported that upregulated transglutaminase 2 (TGase 2) in renal cell carcinoma (RCC) increased HIF-1α and VEGF levels and promoted angiogenesis by inducing p53 degradation. Inhibition of TGase 2 reversed RCC angiogenesis [38]. Chen et al. reported that extracellular vehicles (EVs) derived from fibroblast-like synoviocytes (FLSs) in rheumatoid arthritis (RA) can promote endothelial cell (EC) angiogenesis by targeting the p53/mTOR signaling pathway through miR-1972 [39]. In vitro and in vivo studies have confirmed that p53 can induce miR-1249 to inhibit colorectal cancer (CRC) growth, metastasis, and angiogenesis by targeting VEGFA and HMGA2 [40], indicating that the tumor suppressor p53 activates downstream genes via transcription under stress conditions. In turn, it regulated biological reactions such as the cell cycle, DNA repair, metabolism, angiogenesis, and apoptosis, which was consistent with the results of this study. In the future, it will be necessary to further explore the correlation between ferroptosis markers and angiopoiesis-related factors and to explore the functional changes in trophoblast cells with different p53 expression levels to clarify the specific mechanism by which p53 regulates the SLC7 A11/GPX4 signaling pathway to promote ferroptosis in trophoblast cells during the pathogenesis of PE.

Conclusions

In conclusion, the p53-SLC7 A11/GPX4 system is not only a key mechanism for preventing ferroptosis but also closely related to the pathogenesis of preeclampsia. That is, p53 overexpression inhibited SLC7 A11 activity, and system Xc- synthesis and cysteine transport deficiency mediated OS and lipid ROS accumulation in trophoblast cells. Ferroptosis causes insufficient trophoblast infiltration and poor remodeling or disorder of the uterine spiral artery, which are involved in the occurrence and development of PE. Targeted p53 inhibition can alleviate lipid peroxidation and placental ferroptosis, while promoting angiogenesis. Further study is needed to elucidate the mechanisms and signaling pathways involved in ferroptosis and to gain a deeper understanding of the role of p53-mediated ferroptosis in trophoblast cells in the pathogenesis of PE. This knowledge will provide new insights for basic research and clinical practice on PE with appropriate iron supplementation and tight lipid control, and may lead to novel therapeutic strategies.

Methods

Participant recruitment

Studies have shown that the incidence of preeclampsia in the Chinese population is about 4%. The confidence (Z) was set at 1.96, the significance (α) was set at 0.05, the incidence rate (p) was set at 0.04, according to the formula $n = [Z^2 \times p \times (1 - p)]/\alpha^2$, and the minimum sample size calculated was 59. We enrolled 60 pregnant women who underwent regular obstetric check-ups and who delivered at the Obstetrics Department of Fujian Maternity and Child Health Hospital between September 2022 and December 2023. The participants were divided into two groups: the case group (PE group), consisting of 30 pregnant women with preeclampsia, and the control group (CTL), comprising 30 pregnant women without pregnancy complications. The diagnostic criteria for preeclampsia were based on the ninth edition of Obstetrics and Gynecology published by the People's Health Publishing House [19]. All participants delivered via cesarean section, with those in the PE group undergoing the procedure due to surgical indications. The CTL group had cesarean sections for reasons such as a previous cesarean section, abnormal birth canal, abnormal fetal position, or social factors. Patients with other pregnancies or medical or surgical complications were excluded from the study. Both groups of pregnant women did not have any specific lifestyle habits, such as smoking or alcohol consumption. Informed consent was obtained from all participants through signed consent forms. The experimental procedures were conducted following ethical standards set by local and national human research committees and the principles of the Declaration of Helsinki. Approval for the study protocols was granted by the Ethics Committee of Fujian Maternity and Child Health Hospital (Reference: 2021 KLRD09007) following a review that ensured compliance with relevant regulations, including the "Measures for Ethical Review of Biomedical Research Involving Humans" by the National Health Commission and the Declaration of Helsinki.

Placental sample acquisition

Human placental tissue was collected during cesarean section. Once the placenta had been delivered, we immediately removed a portion of placental villous tissue (1.0 cm^3) from the root of the umbilical cord. We ensured that this procedure was carried out under aseptic conditions and made sure that tissue was only removed from areas on the placenta that did not show bleeding, infarction, or calcification.

Generation of trophoblast cells with different p53 expression levels

The BeWo cells, HTR-8/SVneo cells, and HUVEC used in this study were purchased from Wuhan Punosai Life Technology Co., Ltd and cultured at 37℃ in a 5% CO_2 cell incubator (Thermo Fisher Scientific). The complete medium was prepared as follows: 80–90% Ham's F-12 K medium (Wuhan Punosai Life Technology Co., Ltd) +10–20% common fetal bovine serum (NEWZERUM) +1% double antibody (penicillin/streptomycin) solution (Dalian Meilun Biotechnology Co., Ltd). 80–90% RPMI (1640) basic medium (Dalian Meilun Biotechnology Co., Ltd) +10–20% common fetal bovine serum (NEWZERUM) +1% double antibody (penicillin/streptomycin) solution (Dalian Meilun Biotechnology Co., Ltd); 500 mL ECM basal medium (ScienCell) +25 mL fetal bovine serum (ScienCell) +5 mL endothelial growth factor (ScienCell) +5 mL double antibody (penicillin/streptomycin) solution (ScienCell). Trophoblast cells with different p53 expression levels were constructed as follows:

- p53 overexpression group (p53 +/+): Trophoblast cells were co-cultured with the p53 inducer Nutlin-3 for 72 h.
- p53 inhibition group (p53 −/−): Trophoblast cells were co-cultured with the p53 inhibitor MG-132 for 48 h.
- Control group (CTL): Trophoblast cells were co-cultured with DMSO (dimethyl sulfoxide) for 72 h.

Generation of PE rat models with different p53 expression levels

Female and male Sprague–Dawley rats aged 6–8 weeks and weighing 180 ~ 200 g without a mating history were randomized into four groups of eight rats in each group as follows: (1) p53-overexpressing (p53 +/+) group: before pregnancy, 40 mg/kg of the p53 inducer Nutlin-3 was intraperitoneally injected every 2 days for 14 consecutive days, and 125 mg/kg/day L-NAME was intraperitoneally injected on the 7th day of pregnancy for 7 consecutive days. (2) The inhibition of p53 expression (p53 −/−) group: before pregnancy, the p53 inhibitor MG-132 (10 μg/kg per day) was intraperitoneally injected for 14 consecutive days, and L-NAME (125 mg/kg/day) was intraperitoneally injected for 7 consecutive days on the 7th day of pregnancy; (3) The normal pregnant mouse (CTL) group: before pregnancy, 5 mL of saline was injected intraperitoneally every day for 14 consecutive days, and from the 7th day of pregnancy, 1 mL of normal saline was injected intraperitoneally every day for 7 consecutive days; (4) The preeclampsia pregnant mouse (PE) group: before pregnancy, 5 mL of saline was intraperitoneally injected daily for 14 consecutive days, and 125 mg/kg/day of L-NAME was injected intraperitoneally every day since the 7th day of pregnancy for 7 consecutive days.

Female and male rats were adaptively fed for 1 week. During estrus, male and female rats were fed in the same cage at a ratio of 1:1 so that the date of the discovery of vaginal suppositories or sperm found in vaginal discharge was set as the first day of pregnancy. Random urine samples were collected on the 6th and 19 th days of gestation, blood pressure was measured, and placental tissue was collected on the 20 th day of gestation. After inhalation anesthesia with isoflurane was administered to pregnant rats at 20 th day of gestation, cesarean section was performed to remove the placental tissue and then suture the incision. Approval for the study protocols was granted by the Ethics Committee of Fujian Maternity and Child Health Hospital (Reference: 2021 KLRD09007).

Blood pressure measurement in rats

The blood pressure of the rats was measured by a noninvasive tail artery sphygmomanometer (intelligent noninvasive sphygmomanometer, Beijing Soft Long Biotechnology Co., Ltd.). The pressure sensor was placed on the tail root of the rat, and after the pulse was stable, the start/stop key was pressed to start the measurement. The systolic blood pressure measured by the blood pressure meter should be recorded more than 6 times for each rat (valid data: the average difference between the three consecutive systolic blood pressures in the quiet state of the rat should be the least, and the difference between the three results should be less than 10 mmHg). The mean value was calculated as the systolic blood pressure of the rat on that day, and the whole process was completed within 10 min.

Detection of the urinary protein concentration

The 24-h urinary protein concentration of the rats was measured by the CBB method. The reaction mixture was prepared according to Table 6, and the mixture was thoroughly mixed and incubated for 5 min. After the amount

Table 6 Urinary protein detection reaction system

	Blank tube (mL)	Standard tube (mL)	Measured tube (mL)
Double distilled water	0.05		
563 mg/L protein standard solution		0.05	
Sample			0.05
CBB reagent	3.0	3.0	3.0

of double distilled water was adjusted to zero, the absorbance of each tube was measured at a wavelength of 595 nm and a light diameter of 1 cm. The following formula was used: urinary protein concentration (mg/L) = (measured OD value − blank OD value)/(standard OD value − blank OD value) × standard concentration (563 mg/L).

Detection ROS concentrations in trophoblast cells

The final concentration of DCFH-DA was 10 μM, and the solution was diluted with serum-free medium at 1:1000. The positive control was diluted with serum-free medium at 1:1000 (Rosup, 50 mg/mL) and then added to the cells. DCFH-DA working solution was added, and the cells were incubated at 37 ℃ for 20 ~ 30 min under light protection. The cells were washed with serum-free medium 3 times to fully remove the DCFH-DA that did not enter the cells. The fluorescence intensity before and after stimulation was detected by flow cytometry (BD LSRFortessa™) at an excitation wavelength of 488 nm and an emission wavelength of 525 nm. The concentration of ROS in trophoblast cells is expressed as the mean value of the FITC-A channel.

Determination of the concentration of MDA in placental tissue

The samples were prepared as follows: PBS buffer = 1:10 homogenate lysate placental tissue. The supernatant was collected after centrifugation at 10,000 rpm for 15 min at 4 ℃. The MDA probe was fully dissolved in 5 mL of 95 ℃ ultrapure water and mixed with 5 mL of glacial acetic acid to prepare the MDA probe working solution. According to the number of measured samples (including standard products), the MDA working solution was prepared following Table 7.

A PBS buffer gradient dilution of the MDA standard (200 μM) was used for data analysis via the standard curve method. According to Table 8, the samples were thoroughly mixed with the MDA detection working solution and incubated at 95 ℃ for 40 min.

After being incubated in an ice bath for 5 min, the mixture was centrifuged at 10,000 rpm for 10 min, after which 200 μL of the supernatant was added to a 96-well plate. The absorbance at 532 nm was detected by a BioTek Epoch. The standard curve was drawn according to the gradient dilution standard group-blank group value data:

Table 7 MDA detected working solution

Elements	1 sample	10 samples	50 samples
MDA detected buffers	200 μL	2000 μL	10 mL
MDA probe working solution	200 μL	2000 μL	10 mL
Antioxidant agent	4 μL	40 μL	200 μL

Table 8 MDA working solution

	Standard tube (μL)	Blank tube (μL)	Sample tube (μL)
MDA standard	20		
PBS or H_2O		20	
Sample			20
MDA detected working solution	400	400	400

$Y = aX + b$ (Y is the standard group value − blank group value; X is the MDA concentration of the standard substance; a is the slope of the standard curve; b is the intercept of the standard curve); Unit sample MDA (μmol/gprot) = [(sample group value − blank group value) − b]/a × sample dilution ratio/sample protein concentration (gprot/L).

Determination of the concentration of total iron in placental tissue

Before testing, the reagents in the kit were equilibrated to room temperature. Twenty μl of 10 mmol/L iron standard solution and 1980 μL of double steaming water were mixed evenly. Fresh tissue (0.1 g) was added to 0.9 mL of buffer for homogenization and centrifuged at 10,000 rpm for 10 min, after which the supernatant was collected. Before the formal test, 2 to 3 samples with large expected differences were diluted to different concentrations for the pretest. According to the pretest results, the dilution was carried out in combination with the linear range of the kit (0.4 ~ 50 μmol/L).

Then, 300 μL of the standard solution was added to the corresponding 1.5-mL EP tube as the standard tube. Then, 300 μL of the sample was added to the corresponding 1.5-mL EP tube as the sample tube. Then, 150 μL of chromogenic solution was added and incubated at 37 ℃ for 40 min. After centrifugation at 12,000 rpm for 10 min, 300 μL of the supernatant was added to each corresponding well of the enzyme label plate, and the OD of each well was measured at 593 nm with a BioTek Epoch. Standard fitting curve: $y = ax + b$; y: standard solution OD value − blank OD value (OD value when standard solution concentration is 0); a: slope of the mark; x: concentration of standard solution; b: intercept of the mark; Tissue total iron content (μmol/kg wet weight) = $(\triangle A - b)/a \times f/(m/V)$; $\triangle A$: the absolute OD value of the sample (OD value of the determination hole − OD value of the control hole); b: intercept of the mark; a: slope of the mark; f: dilution ratio of the sample before adding to the test system; m: sample homogenate quality (g); V: amount of sample homogenate added (mL).

Morphological observation of trophoblast cells in placental tissue

Fresh placental tissue (no more than 1 mm × 1 mm × 1 mm) was fixed in electron microscope fixative solution at 4 ℃ for 2 ~ 4 h and then rinsed with 0.1 M phosphate buffer (pH 7.4) 3 times for 15 min each. After the addition of 1% osmic acid · 0.1 M phosphate buffer, PB (pH 7.4) was fixed at room temperature (20℃) for 2 h and then rinsed with 0.1 M phosphate buffer PB (pH 7.4) 3 times for 15 min each. The samples were dehydrated in 50%–70%–80%–90%–95%–100%–100% alcohol–100%–100% acetone for 15 min each. The samples were transferred to acetone:812 embedding agent = 1:1 for 2 ~ 4 h, acetone:812 embedding agent = 1:2 overnight, and pure 812 embedding agent = 5 ~ 8 h. Pure 812 embedding agent was poured into the embedding plate, which was then placed in an oven at 37 ℃ overnight. The samples were polymerized in an oven at 60 °C for 48 h. Ultrathin Sects. (60 ~ 80 nm) were then prepared using a Leica UC7 ultrathin microtome. Sections were double stained with uranium lead (2% uranium acetate saturated alcohol solution and lead citrate for 15 min each) and dried overnight at room temperature. Images were acquired and analyzed using a transmission electron microscope (HT7700; HITACHI).

Quantitative real-time PCR (qRT–PCR)

The 50 mg sample was fully ground, mixed with 1 mL of TRIzol and left for 5 min. Then, 200 μL of chloroform was added, and the mixture was shaken for 15 s. The mixture was left for 5 min and centrifuged at 12,000 rpm at 4℃ for 15 min. Then, 500 μL of the supernatant was removed, 500 μL of isopropyl alcohol was added (supernatant:isopropyl alcohol = 1:1), the mixture was allowed to stand for 5 min, and the mixture was centrifuged at 12,000 rpm at 4℃ for 10 min. The supernatant was discarded, 600 μL of 75% ethanol (anhydrous ethanol:DEPC-treated water = 3:1) was added, the precipitate was oscillated, and the precipitate was washed and centrifuged at 12,000 rpm at 4℃ for 5 min (this process was repeated 3 times). The supernatant was discarded, and the total RNA was dissolved in 30 μL of DEPC-treated water. The concentration and purity of the RNA were determined with a Thermo Scientific spectrophotometer.

The reverse transcription kit used in this study was purchased from TaKaRa's TB Green® Premix Ex Taq™ (Tli RNaseH Plus). According to the reaction system of SYBR® Green analysis, 500 ng of total RNA was needed, and the required RNA volume was calculated as VRNA = $500/C_{RNA}$ (μL). Total RNA was used as a template, and the reverse transcription reaction solution was prepared on ice according to Table 9. The solution was centrifuged and mixed on a thermal cycler at (1) 37℃ for 15 min, (2) 85℃ for 15 s, and (3) 4℃ for reverse transcription.

The primers used in this study were synthesized by Fuzhou Shangya Biological Co., Ltd (Table 10). The PCR kit used in this study was purchased from the PrimeScriptTM RT Reagent Kit (Perfect Real Time) of TaKaRa Company in Japan. The PCR solution was prepared on ice according to Table 11.

The solution was centrifuged and then placed on a Quant Studio 3 fluorescence quantitative PCR instrument. The reaction conditions were as follows: (1) 95℃ for 30 s; (2) 95℃ for 5 s; 60℃ for 34 s for 40 cycles; (3) 95℃ for 15 s; 60℃ for 1 min; and 95℃ for 15 s. The mRNA level of GAPDH was used as the control, and the relative mRNA expression was calculated as $2^{-\triangle\triangle CT}$ [△△CT = experimental group (objective CT-internal reference CT) − control group (objective CT-internal reference CT)].

Table 10 Primer information

Target gene	Primer sequence
GAPDH	F: 5′-ACGGCAAGTTCAACGGCACAG-3′ R: 5′-GAAGACGCCAGTAGACTCCACGAC-3′
p53	F: 5′-CAGCACATGACGGAGGTTGT-3′ R: 5′-TCTCCAAATACTCCACAGC-3′
SLC7 A11	F: 5′-CCTGTTTGTCCACCATTC-3′ R: 5′-GATGAA GATTCCTCTCCAATGA-3′
GPX4	F: 5′-GAGGCAAACGGAAGTAAACTAC-3′ R: 5′-CCG AACTGGTTACACGGGAA-3′

Table 9 Reverse transcriptional reaction solution

Reagent	Amount (μL)
5 × PrimeScript Buffer	4
PrimeScript RT Enzyme Mix I	1
Oligo dT Primer (50 μM)	1
Random 6 mers (100 μM)	1
Total RNA	
RNase Free dH_2O	up to 20

Table 11 PCR reaction solution

Reagent	Amount (μL)
SYBR Premix Ex Taq	30.0
PCR Forward Primer (10 μM)	1.2
PCR Reverse Primer (10 μM)	1.2
cDNA	6.0
dH_2O	21.4
Total	60.0

Western blot (WB)

One hundred milligrams of sample tissue was added to 1000 μL of freshly prepared protein lysate (RIPA lysis buffer containing the protease inhibitor PMSF = 100:1, ice operation) for cleavage. The samples were centrifuged at 12,000 rpm at 4℃ for 10 min. A BCA protein quantitative/concentration assay kit (Dalian Meilun Biotechnology Co., Ltd.) was used to determine the concentration of each protein sample. Then, 5× SDS protein loading buffer was added, and the samples were incubated in a 100℃ water bath for 10 min for denaturation. Then, 50 μg of protein sample (Vprotein = 50/Cprotein/0.8) and 5 μL of protein marker were added to the lanes. After 40 min of electrophoresis at a constant voltage of 80 V, the voltage was adjusted to 120 V to continue electrophoresis. The film transfer device was installed, and the film transfer conditions were set at 70 V for 90 min. After membrane transfer, the PVDF membrane was shaken and washed three times with TBST buffer for 10 min each. Fresh 5% skim milk powder sealing solution was added, and the membrane was slowly shaken at room temperature for 2 h. After the membrane was blocked with TBST, the membrane was washed with TBST for 10 min, and this process was repeated three times. The PVDF membrane was placed into a container containing primary antibody solution (Immunoway) (antibody: primary antibody diluent = 1:1000) and incubated in a shaking bed slowly at 4℃ overnight (12 ~ 16 h). After incubation with the primary antibody, the PVDF membrane was washed with TBST for 10 min on a shaker, and this process was repeated three times. The PVDF membrane was placed into a container containing a secondary antibody solution (Immunoway) (antibody: secondary antibody diluent = 1:1000) and incubated in a shaker at room temperature for 1 h. After incubation, the PVDF membrane was washed with TBST buffer for 10 min, and this process was repeated three times. The developing solution was prepared by mixing liquid A and liquid B in a hypersensitive enhanced chemiluminescence (ECL) kit (Dalian Meilun Biotechnology Co., Ltd.) at a 1:1 ratio. The PVDF membrane was immersed in developing solution for 30 s and then photographed with an automatic Western blot imaging analyzer (Fluor Chem M). The gray values of the protein bands were analyzed by Image Lab image analysis software. The relative protein expression was calculated as the gray value of the target protein/gray value of the internal reference protein.

Immunohistochemistry (IHC)

The sections were sequentially washed with 15 min of dewaxing solution I, 15 min of dewaxing solution II, 15 min of dewaxing solution III, 15 min of anhydrous ethanol I, 5 min of anhydrous ethanol II, 5 min of 85% alcohol, 5 min of 75% alcohol, and 5 min of distilled water. The sections were placed in citric acid antigen repair buffer (pH 6.0) in a repair box for antigen repair in a microwave oven, heated for 8 min to boiling, allowed to cool for 8 min to warm and then returned to medium and then to low heat for 7 min. After natural cooling, the sections were placed in PBS (pH 7.4) buffer on a shaker and washed 3 times for 5 min each. The sections were incubated in 3% hydrogen peroxide solution at room temperature for 25 min and then washed. The tissue was uniformly covered with 3% BSA and incubated at room temperature for 30 min. Primary antibody diluent was added to the sections, which were then placed in a wet box at 4 °C overnight incubation before washing. The tissue was covered with secondary antibody diluent, incubated at room temperature for 50 min and then washed. DAB developing solution was added to the sections, and the color development time was controlled under a microscope. The sections were rinsed with tap water to terminate color development. The sections were redyed with hematoxylin for 3 min and then washed with tap water. After differentiation, the sections were washed with hematoxylin differentiation solution and tap water for a few seconds. After the sections were rinsed with blue return water, they were rinsed with hematoxylin blue solution. The sections were incubated in 75% alcohol for 5 min, 85% alcohol for 5 min, anhydrous ethanol I for 5 min, anhydrous ethanol II for 5 min, and n-butanol for 5 min, followed by xylene I for 5 min, after which they were dried and sealed with neutral gum.

Microscopy, image acquisition, and analysis

Immunofluorescence and confocal laser technology

The sections were subsequently washed in xylene I 15 min-xylene II 15 min-anhydrous ethanol I 5 min-anhydrous ethanol II 5 min-85% alcohol 5 min-75% alcohol 5 min-distilled water. The sections were placed in EDTA antigen repair buffer (pH 8.0) and subjected to antigen retrieval in a microwave oven. The medium was heated for 8 min, the fire was stopped for 8 min, and the medium was changed to low heat for 7 min. After natural cooling, the sections were placed in PBS (pH 7.4) and shaken 3 times for 5 min each. The sections were placed in 3% hydrogen peroxide solution, incubated for 25 min at room temperature in the dark and then washed. The sections were blocked with BSA for 30 min. Primary antibody diluent was added to the sections, which were then incubated in a wet box at 4 °C overnight and washed. The secondary antibody diluent was added to the sections, which were incubated at room temperature for 50 min and then washed. CY3-TSA was added to the sections, which were incubated at room temperature for 10 min

and then washed. The sections were placed in an EDTA antigen repair buffer (pH 8.0) repair box and heated in a microwave oven. The medium was heated for 8 min, the temperature was stopped for 8 min and the medium was changed to low heat for 7 min. The second primary antibody diluent was added to the sections, which were incubated in a wet box at 4 °C overnight and then washed. The secondary antibody diluent was added to the sections, which were incubated at room temperature for 50 min and then washed. The TSA was added to the sections, which were incubated at room temperature for 10 min in the dark and then washed. The sections were placed in an EDTA antigen repair buffer (pH 8.0) repair box and heated in a microwave oven. The medium was heated for 8 min, the temperature was stopped for 8 min, and the medium was changed to low heat for 7 min. The third primary antibody diluent was added to the section, which was incubated in a wet box at 4 °C overnight and then washed. Then, Cy5-labeled fluorescent secondary antibody diluent was added to the sections, which were incubated at room temperature for 50 min in the dark and then washed. DAPI dye solution was added to the sections, which were incubated at room temperature for 10 min in the dark and then washed. The autofluorescence quencher was added to the sections for 5 min, and the sections were rinsed with running water for 10 min and then washed. The sections were sealed with antifluorescence quenching solution. The sections were placed under a scanner to capture images.

ELISA

The sample was centrifuged at 5000 rpm for 5 min, after which the supernatant was collected. The standard product was successively diluted to 1000, 500, 250, 125, 62.5, 31.2, 15.6, and 0 pg/mL. Solution A and solution B were diluted 1:100. The thick washing solution was diluted 30 times. After 100 μL of standard or sample solution was added, the enzyme-labeled plate was coated and incubated at 37℃ for 2 h. The liquid in the hole was discarded, 100 μL of detection solution A was added, and the enzyme-labeled plate was incubated at 37℃ for 1 h. The liquid in the hole was discarded, and the plate was washed 3 times with 350μL of washing liquid. The detection solution B working solution (100 μL) was added, and the enzyme-labeled plate was incubated at 37℃ for 30 min. The liquid in the well was discarded, and the plate was washed 5 times. Next, 90 μL of TMB substrate solution was added, the plate was coated, and the color was developed at 37℃ in the dark. When the gradient of blue was obvious in the first 3 to 4 holes of the standard hole, the gradient of the last 3 to 4 holes was not obvious, and the process could be terminated. Then, 50 μL of termination solution was added to terminate the reaction. The optical density of each well was immediately measured with a BioTek Epoch at a wavelength of 450 nm.

Angiogenesis test

The matrix glue was melted overnight, and the 200 μL pipette head and 48-well plate were precooled in advance. Then, 150 μL of matrix glue was added to the 48-well plate and incubated in a cell incubator at 37℃ for 30 min. The HUVEC suspension was prepared at a density of 1×10^5/mL. According to the groups, 500 μL of cell suspension was added to each of the coated plates and incubated at 37℃ for 3 ~ 4 h. After incubation, endothelial cell canalization was observed under an inverted microscope (Nikon), and angiogenesis was quantified in 3 random fields to analyze the relevant data.

Statistical analysis

All the data were statistically analyzed with the SPSS 26.0 software package. The measurement data are expressed as the mean ± standard deviation (SD). One-way analysis of variance (ANOVA) and the least significant difference (LSD) test were used to compare the differences among multiple groups. The independent samples *t*-test was used to compare two groups. When the test level was $\alpha = 0.05$, $P < 0.05$ was considered to indicate a statistically significant difference.

Abbreviations

BMI	Body mass index
system Xc-	Cysteine/glutamate antiporter
DP	Diastolic blood pressure
EOPE	Early-onset preeclampsia
FT1	Ferritin 1
FTH1	Ferritin heavy 1
GDM	Gestational diabetes mellitus
GSH	Glutathione
GPX4	Glutathione peroxidase 4
HUVECs	Human umbilical vein endothelial cells
HIF-1α	Hypoxia-inducible factor 1α
LOPE	Late-onset preeclampsia
LPO	Lipide peroxide
MDA	Malondialdehyde
MDM2	Murine double minute 2
OS	Oxidative stress
PUFAs	Polyunsaturated fatty acids
PE	Preeclampsia
ROS	Reactive oxygen species
SLC7 A11	Solute carrier family 7, member 11
SP	Systolic blood pressure
VEGF	Vascular endothelial growth factor

Supplementary Information

The online version contains supplementary material available at https://doi.org/10.1186/s12915-025-02240-9.

Supplementary Material 1

Acknowledgements
We would like to thank the EditSprings (https://www.editsprings.cn/) for the expert linguistic services provided.

Authors' contributions
Material preparation, data collection and analysis were performed by TTL, XX, GYW and JYY. As TTL and XX contributed equally to the article, we decided to list them as co-first authors. The first draft of the manuscript was written by TTL, XX, GYW and JYY and all authors commented on previous versions of the manuscript. All authors read and approved the final manuscript.

Funding
This research was funded by Fujian Provincial Health Technology Project (2024ZD01005); Joint Funds for the Innovation of Science and Technology, Fujian Province (2020Y9134); National Key Clinical Specialty Construction Program of China (Obstetric); Fujian Provincial Natural Science Foundation of China (2024Y0035); Joint Funds for the Innovation of Science and Technology, Fujian Province (2024Y9536); Startup Fund for Scientific Research, Fujian Medical University (2023QH2046).

Data availability
No datasets were generated or analysed during the current study.

Declarations

Ethics approval and consent to participate
Ethical approval was obtained from the Ethics Committee of Fujian Maternity and Child Health Hospital (Reference: 2021 KLRD09007).

Consent for publication
We agree to publish this article.

Competing interests
The authors declare no competing interests.

Author details
[1]College of Clinical Medicine for Obstetrics & Gynecology and Pediatrics, Fujian Medical University Fujian Maternity and Child Health Hospital, Fujian Clinical Research Center for Maternal-Fetal Medicine, Laboratory of Maternal-Fetal Medicine, Fujian Maternity and Child Health Hospital, National Key Obstetric Clinical Specialty Construction Institution of China, No. 18, Daoshan Road, Gulou District, Fuzhou, Fujian Province, China.

Received: 18 February 2025 Accepted: 9 May 2025
Published online: 28 May 2025

References

1. Marzioni D, Piani F, Di Simone N, et al. Importance of STAT3 signaling in preeclampsia (Review)[J]. Int J Mol Med. 2025;55(4):58.
2. Annesi L, Tossetta G, Borghi C, et al. The Role of Xanthine Oxidase in Pregnancy Complications: A Systematic Review[J]. Antioxidants (Basel). 2024;13(10):1234.
3. Piani F, Agnoletti D, Baracchi A, et al. Serum uric acid to creatinine ratio and risk of preeclampsia and adverse pregnancy outcomes[J]. J Hypertens. 2023;41(8):1333–8.
4. Raguema N, Moustadraf S, Bertagnolli M. Immune and Apoptosis Mechanisms Regulating Placental Development and Vascularization in Preeclampsia[J]. Front Physiol. 2020;11:98.
5. Lei G, Mao C, Yan Y, et al. Ferroptosis, radiotherapy, and combination therapeutic strategies[J]. Protein Cell. 2021;12(11):836–57.
6. Ji X, Qian J, Rahman SMJ, et al. xCT (SLC7A11)-mediated metabolic reprogramming promotes non-small cell lung cancer progression[J]. Oncogene. 2018;37(36):5007–19.
7. Guerby P, Tasta O, Swiader A, et al. Role of oxidative stress in the dysfunction of the placental endothelial nitric oxide synthase in preeclampsia[J]. Redox Biol. 2021;40: 101861.
8. Xie Y, Hou W, Song X, et al. Ferroptosis: process and function[J]. Cell Death Differ. 2016;23(3):369–79.
9. Chen X, Liu C, Yu R, et al. Interaction between ferroptosis and TNF-α: Impact in obesity-related osteoporosis[J]. FASEB J. 2023;37(6): e22947.
10. Gumilar KE, Priangga B, Lu CH, et al. Iron metabolism and ferroptosis: A pathway for understanding preeclampsia[J]. Biomed Pharmacother. 2023;167: 115565.
11. Mégier C, Peoc'h K, Puy V, et al. Iron Metabolism in Normal and Pathological Pregnancies and Fetal Consequences[J]. Metabolites. 2022;12(2):129.
12. Marei HE, Althani A, Afifi N, et al. p53 signaling in cancer progression and therapy[J]. Cancer Cell Int. 2021;21(1):703.
13. Madrigal T, Hernández-Monge J, Herrera LA, et al. Regulation of miRNAs Expression by Mutant p53 Gain of Function in Cancer[J]. Front Cell Dev Biol. 2021;9: 695723.
14. Bao D, Zhuang C, Jiao Y, et al. The possible involvement of circRNA DMNT1/p53/JAK/STAT in gestational diabetes mellitus and preeclampsia[J]. Cell Death Discov. 2022;8(1):121.
15. Zhang Z, Guo M, Shen M, et al. The BRD7-P53-SLC25A28 axis regulates ferroptosis in hepatic stellate cells[J]. Redox Biol. 2020;36: 101619.
16. Qi SM, Cheng G, Cheng XD, et al. Targeting USP7-Mediated Deubiquitination of MDM2/MDMX-p53 Pathway for Cancer Therapy: Are We There Yet?[J]. Front Cell Dev Biol. 2020;8:233.
17. Yang Z, Li H, Luo P, et al. UNC5B Promotes Vascular Endothelial Cell Senescence via the ROS-Mediated P53 Pathway[J]. Oxid Med Cell Longev. 2021;2021:5546711.
18. Pfaff MJ, Mukhopadhyay S, Hoofnagle M, et al. Tumor suppressor protein p53 negatively regulates ischemia-induced angiogenesis and arteriogenesis[J]. J Vasc Surg. 2018;68(6S):222S-233S.e1.
19. Xing X, Beihua K, Tao D, et al. Obstetrics and Gynecology. 9th ed. Beijing: People's Medical Publishing House; 2018.
20. Colson A, Sonveaux P, Debiève F, et al. Adaptations of the human placenta to hypoxia: opportunities for interventions in fetal growth restriction[J]. Hum Reprod Update. 2021;27(3):531–69.
21. Staff AC. The two-stage placental model of preeclampsia: An update[J]. J Reprod Immunol. 2019;134–135:1–10.
22. Rana S, Lemoine E, Granger JP, et al. Preeclampsia: Pathophysiology, Challenges, and Perspectives[J]. Circ Res. 2019;124(7):1094–112.
23. Schoots MH, Gordijn SJ, Scherjon SA, et al. Oxidative stress in placental pathology[J]. Placenta. 2018;69:153–61.
24. Zhang H, He Y, Wang JX, et al. miR-30-5p-mediated ferroptosis of trophoblasts is implicated in the pathogenesis of preeclampsia[J]. Redox Biol. 2020;29: 101402.
25. Xu X, Zhu M, Zu Y, et al. Nox2 inhibition reduces trophoblast ferroptosis in preeclampsia via the STAT3/GPX4 pathway[J]. Life Sci. 2024;343: 122555.
26. Liao T, Xu X, Ye X, Yan J. DJ-1 upregulates the Nrf2/GPX4 signal pathway to inhibit trophoblast ferroptosis in the pathogenesis of preeclampsia. Sci Rep. 2022;12(1):2934.
27. Dixon SJ, Lemberg KM, Lamprecht MR, et al. Ferroptosis: an iron-dependent form of nonapoptotic cell death[J]. Cell. 2012;149(5):1060–72.
28. Su LJ, Zhang JH, Gomez H, et al. Reactive Oxygen Species-Induced Lipid Peroxidation in Apoptosis, Autophagy, and Ferroptosis[J]. Oxid Med Cell Longev. 2019;2019:5080843.
29. Burton GJ, Cindrova-Davies T, Yung HW, et al. HYPOXIA AND REPRODUCTIVE HEALTH: Oxygen and development of the human placenta[J]. Reproduction. 2021;161(1):F53–65.
30. Yang N, Wang Q, Ding B, et al. Expression profiles and functions of ferroptosis-related genes in the placental tissue samples of early- and late-onset preeclampsia patients[J]. BMC Pregnancy Childbirth. 2022;22(1):87.
31. Chiang YT, Chien YC, Lin YH, et al. The Function of the Mutant p53–R175H in Cancer[J]. Cancers (Basel). 2021;13(16):4088.
32. Bebber CM, Müller F, Prieto Clemente L, et al. Ferroptosis in Cancer Cell Biology[J]. Cancers (Basel). 2020;12(1):164.
33. Kirtonia A, Sethi G, Garg M. The multifaceted role of reactive oxygen species in tumorigenesis[J]. Cell Mol Life Sci. 2020;77(22):4459–83.
34. Guan Z, Chen J, Li X, et al. Tanshinone IIA induces ferroptosis in gastric cancer cells through p53-mediated SLC7A11 down-regulation[J]. Biosci Rep. 2020;40(8):BSR20201807.
35. Ma S, Sun L, Wu W, et al. USP22 Protects Against Myocardial Ischemia-Reperfusion Injury via the SIRT1-p53/SLC7A11-Dependent Inhibition

of Ferroptosis-Induced Cardiomyocyte Death[J]. Front Physiol. 2020;11: 551318.
36. Men H, Cai H, Cheng Q, et al. The regulatory roles of p53 in cardiovascular health and disease[J]. Cell Mol Life Sci. 2021;78(5):2001–18.
37. Ma XL, Li XC, Tian FJ, et al. Effect of the p53-tristetraprolin-stathmin-1 pathway on trophoblasts at maternal-fetal interface[J]. PLoS ONE. 2017;12(6):e0179852.
38. Lee SH, Kang JH, Ha JS, et al. Transglutaminase 2-Mediated p53 Depletion Promotes Angiogenesis by Increasing HIF-1α-p300 Binding in Renal Cell Carcinoma[J]. Int J Mol Sci. 2020;21(14):5042.
39. Chen Y, Dang J, Lin X, et al. RA Fibroblast-Like Synoviocytes Derived Extracellular Vesicles Promote Angiogenesis by miRNA-1972 Targeting p53/mTOR Signaling in Vascular Endotheliocyte[J]. Front Immunol. 2022;13: 793855.
40. Chen X, Zeng K, Xu M, et al. P53-induced miR-1249 inhibits tumor growth, metastasis, and angiogenesis by targeting VEGFA and HMGA2[J]. Cell Death Dis. 2019;10(2):131.

Publisher's Note